Bioconjugate Chemistry

Article

pubs.acs.org/bc

Enhancing PET Signal at Target Tissue in Vivo: Dendritic and Multimeric Tris(hydroxypyridinone) Conjugates for Molecular Imaging of $\alpha_v\beta_3$ Integrin Expression with Gallium-68

Cinzia Imberti,[†] Samantha Y. A. Terry,[†] Carleen Cullinane,[‡,§] Fiona Clarke,[∥] Georgina H. Cornish,[∥] Nisha K. Ramakrishnan,[†] Peter Roselt,[‡] Andrew P. Cope,[∥] Rodney J. Hicks,[‡,§] Philip J. Blower,[†] and Michelle T. Ma*[,†]

[†]King's College London, Division of Imaging Sciences and Biomedical Engineering, Fourth Floor Lambeth Wing, St Thomas' Hospital, London SE1 7EH, United Kingdom

[‡]Peter MacCallum Cancer Centre, Melbourne, Victoria 3000, Australia

[§]Sir Peter MacCallum Department of Oncology, University of Melbourne, Parkville, Victoria 3010, Australia

[∥]King's College London, Academic Department of Rheumatology, Centre for Molecular and Cellular Biology of Inflammation, Faculty of Life Sciences and Medicine, London SE1 1UL, United Kingdom

Supporting Information

ABSTRACT: Tris(hydroxypyridinone) chelators conjugated to peptides can rapidly complex the positron-emitting isotope gallium-68 (^{68}Ga) under mild conditions, and the resulting radiotracers can delineate peptide receptor expression at sites of diseased tissue in vivo. We have synthesized a dendritic bifunctional chelator containing nine 1,6-dimethyl-3-hydroxypyridin-4-one groups (SCN-HP$_9$) that can coordinate up to three Ga^{3+} ions. This derivative has been conjugated to a trimeric peptide (RGD$_3$) containing three peptide groups that target the $\alpha_v\beta_3$ integrin receptor. The resulting dendritic compound, HP$_9$-RGD$_3$, can be radiolabeled in 97% radiochemical yield at a 3-fold higher specific activity than its homologues HP$_3$-RGD and HP$_3$-RGD$_3$ that contain only a single metal binding site. PET scanning and biodistribution studies show that [^{68}Ga(HP$_9$-RGD$_3$)] demonstrates higher receptor-mediated tumor uptake in animals bearing U87MG tumors that overexpress $\alpha_v\beta_3$ integrin than [^{68}Ga(HP$_3$-RGD)] and [^{68}Ga(HP$_3$-RGD$_3$)]. However, concomitant nontarget organ retention of [^{68}Ga(HP$_9$-RGD$_3$)] results in low tumor to nontarget organ contrast in PET images. On the other hand, the trimeric peptide homologue containing a single tris(hydroxypyridinone) chelator, [^{68}Ga(HP$_3$-RGD$_3$)], clears nontarget organs and exhibits receptor-mediated uptake in mice bearing tumors and in mice with induced rheumatoid arthritis. PET imaging with [^{68}Ga(HP$_3$-RGD$_3$)] enables clear delineation of $\alpha_v\beta_3$ integrin receptor expression in vivo.

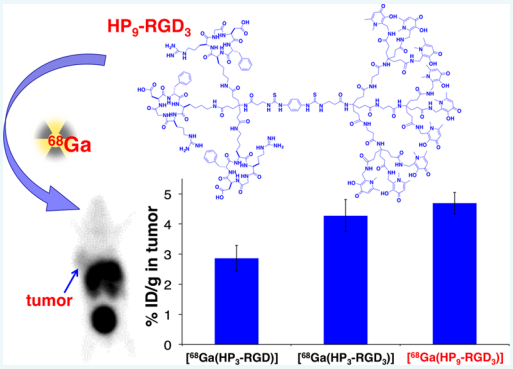

INTRODUCTION

Peptide-based imaging agents in nuclear medicine have tremendous utility in diagnosis, prognosis, and selection of therapeutic regimes for patients. Radiometals can be incorporated into clinically relevant peptides via a bifunctional chelator, providing effective and sensitive radiotracers that can be prepared conveniently in a radiopharmacy. The metallic isotope ^{68}Ga possesses decay properties that are suitable for positron emission tomography (PET) (68 min half-life, 1899 keV β^+ emission with 88% abundance), and the availability of a pharmaceutical grade ^{68}Ge/^{68}Ga generator means that the number of molecular imaging agents based on ^{68}Ga is likely to increase in the coming years. The somatostatin receptor 2-targeted imaging agent, ^{68}Ga-DOTATATE for neuroendocrine tumors,[1−3] and more recently, the prostate specific membrane antigen targeted conjugate, ^{68}Ga-HBED-PSMA,[4,5] have demonstrated clinical utility in patient prognosis and management. Other chelator systems have exhibited efficient $^{68}Ga^{3+}$ radiolabeling properties, and the resulting radiolabeled conjugates are effective at delineating target tissue in vivo.[6−12] Among these are the tripodal tris(hydroxypyridinone) chelators containing three 1,6-dimethyl-3-hydroxypyridin-4-one groups that can coordinate radiometallic Ga^{3+} and Zr^{4+} ions,[13−15] as well as Fe^{3+} and Al^{3+} with high affinity.[16,17] Upon deprotonation of hydroxyl groups, the hexadentate O_6 ligand, THP-Ac, can coordinate $^{68}Ga^{3+}$ at mild pH (pH 6.5−7.5) and low ligand concentrations (10 μM) in <5 min.[13] Bifunctional derivatives of THP-Ac can be attached to peptides, with the

Received: October 26, 2016
Revised: November 23, 2016
Published: November 29, 2016

DOI: 10.1021/acs.bioconjchem.6b00621
Bioconjugate Chem. 2017, 28, 481−495

Chart 1

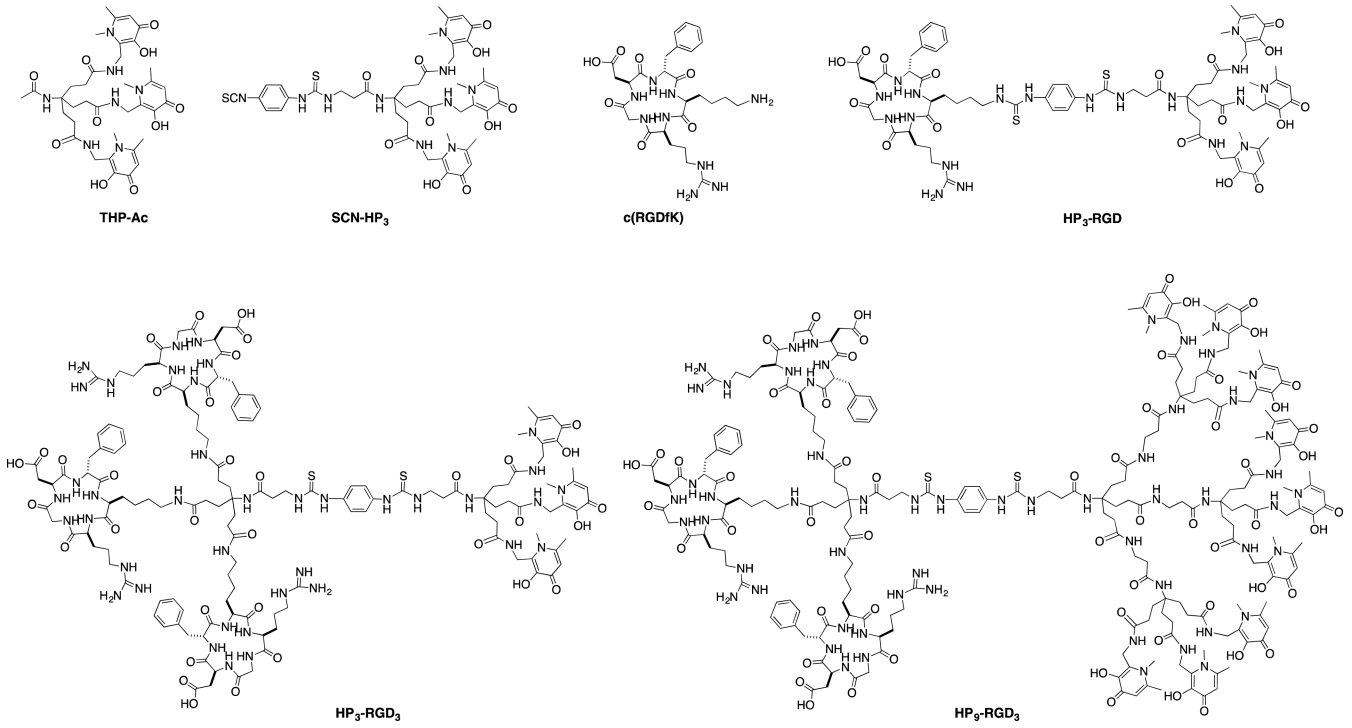

resulting conjugates able to rapidly and quantitatively coordinate aqueous $^{68}Ga^{3+}$ at room temperature at pH 5−7.[18,19]

Multimeric peptide-based imaging agents that incorporate more than one peptide targeting group (and in particular small peptides that target the $\alpha_v\beta_3$ integrin receptor) have demonstrated increased accumulation of activity at tissue targets in vivo relative to their monomeric analogues, and are effective contrast agents.[8,12,20−27] This increased accumulation of radiotracer in the case of multimeric compounds can be attributed to either (i) divalent binding, where two targeting peptides bind to two receptors simultaneously, requiring sufficient distance between the two intramolecular targeting ligands to form this bridge; or (ii) an increased local effective concentration of targeting peptide at the receptor site, resulting in a shift in equilibrium toward peptide receptor binding. In the case where the multimeric derivative has an increased persistence in the blood pool in vivo relative to the monomeric derivative, it is also possible that increased uptake is a result of increased bioavailability.

Dendritic and multimeric chelator systems for coordination of Gd^{3+} and lanthanides provide enhanced contrast as MRI agents compared to their single-chelator counterparts, in large part due to the increased number of metal complexes present.[28−36] Multimeric constructs containing multiple chelating groups (including hydroxypyridinones) have also been synthesized for the purposes of sequestering trace metal ions.[17,37] A small body of work has been described in which the number of radiometal coordination sites on a radiolabeled protein/antibody has been increased by incorporation of either a dendrimer possessing multiple chelating groups,[38−41] or a pendant function (such as polylysine) on which multiple chelators are appended.[42−44] In these cases, the functionalized/radiolabeled biomolecule retained affinity for receptor targets in vitro[40,41,44] and in vivo.[38,39,42,43] Additionally, when compared to bioconjugates containing fewer chelating groups, dendrimer or multichelator conjugated proteins demonstrated higher specific activity—that is, a higher number of radionuclides were bound per bioconjugate compared to homologues containing a single chelator.[38,41−43] In some cases, this resulted in higher concentrations of radioactivity at target tissue (tumors) in vivo.[42]

We are interested in using tris(hydroxypyridinone) ligands to explore new ways of increasing accumulated radioactivity at diseased tissue where target receptors are localized in vivo. Here we aim to incorporate multiple in vivo targeting peptide groups and multiple chelator groups into a single molecule, thus increasing the affinity of the radiolabeled conjugate for receptors in vivo as well as increasing the specific activity of the radiolabeled species itself. This approach mimics that of multifunctionalized nanoparticles, where multiple copies of a targeting biomolecule/modifying agent and multiple chelating groups are appended to the surface of a nanoparticle.[45−48] We have employed the cyclic pentapeptide, c(RGDfK), (Chart 1) that targets the endothelial $\alpha_v\beta_3$ integrin receptor expressed in angiogenesis, and is associated with metastatic disease in cancers. The biology of such conjugates is well understood, and derivatives of c(RGDfK) are useful model compounds for assessing novel approaches to molecular imaging using peptide-based agents.

We have synthesized a novel bifunctional chelator construct that incorporates three hexadentate tris(hydroxypyridinone) metal binding sites for Ga^{3+} and an isothiocyanate group that can be utilized as an attachment point to lysine residues of the N-terminus of peptides. We have also employed a scaffold for facile attachment of three c(RGDfK) peptide targeting groups that contain available Lys or N-terminal primary amine groups, ultimately providing a trimeric targeting motif. Conjugating these two motifs together results in a dendritic compound where an aryl group links a trimeric peptide targeting group and three tris(hydroxypyridinone) (THP) groups. We have also synthesized homologues of this compound to investigate the

DOI: 10.1021/acs.bioconjchem.6b00621
Bioconjugate Chem. 2017, 28, 481−495

Scheme 1. Synthesis of SCN-HP$_9$

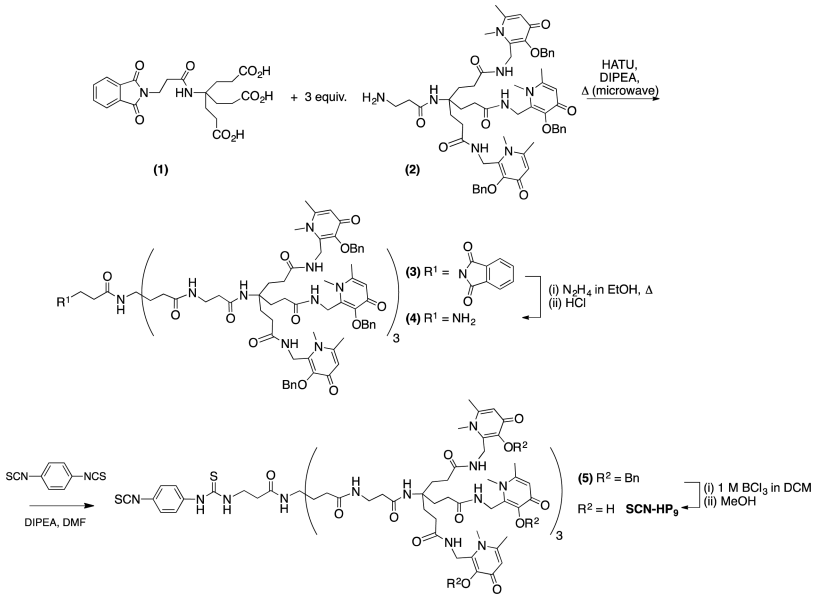

effect of incorporating multiple copies of a peptide/chelating group on in vitro uptake and in vivo biodistribution and target tissue accumulation. Finally, we have chosen the radiotracer with the best in vivo tumor to nontarget organ contrast and assessed the radiotracer in a model of rheumatoid arthritis to further illustrate the utility of ^{68}Ga-labeled THP conjugates that target integrin receptors for molecular imaging of in vivo events.

RESULTS

Synthesis. To synthesize a multidentate chelator containing nine 1,6-dimethyl-3-hydroxypyridin-4-one groups (as three tris(hydroxypyridinone) moieties), the benzyl-protected tris-(hydroxypyridinone) (**2**) (3 equiv) was reacted with tricarboxylate (**1**), HATU, and diisopropylethylamine under microwave conditions (Scheme 1). The resulting compound (**3**) was purified using silica chromatography. Subsequent removal of the phthalimide group furnished **4**, which possesses a primary amine that can be further functionalized for attachment to biomolecules. This species was converted to a phenyl isothiocyanate by reacting it with an excess of *p*-phenylene diisothiocyanate, resulting in **5**, which was isolated via semipreparative reverse phase HPLC. Compound SCN-HP$_9$ was obtained upon deprotection of the benzyl-protected hydroxypyridinone groups by reaction of **5** with boron trichloride in dichloromethane, followed by addition of methanol.

This study aimed to assess a trimeric scaffold in which all three peptide motifs are equidistant from the bifunctional chelator and chemically equivalent to each other, thus ensuring that all three motifs possess the same affinity for the target receptor. To achieve this, tricarboxylate **1** was converted to a *N*-hydroxysuccinimide-activated intermediate (**6**) which was reacted with 3 equiv of c(RGDfK), to provide the multimeric compound **7**. Compound **7** was purified and isolated using RP-HPLC. The phthalimide group was removed by reaction with hydrazine in ethanol, followed by addition of HCl (Scheme 2). Subsequently, RGD$_3$, which contains three c(RGDfK) peptide groups and an apical primary amine, was isolated using RP-HPLC.

Scheme 2. Synthesis of RGD$_3$

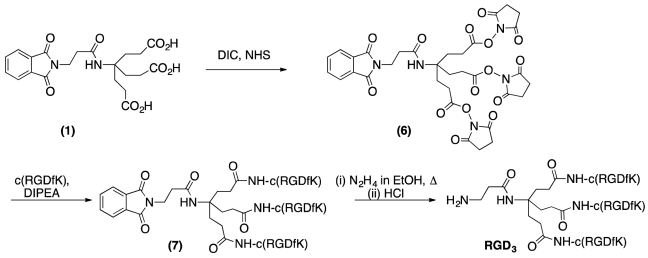

Reaction of RGD$_3$ with SCN-HP$_9$ at 120 °C at 300 W in a microwave reactor provided HP$_9$-RGD$_3$ (Chart 1) which was purified and isolated using RP-HPLC in ≥95% purity. HP$_9$-RGD$_3$ possesses three c(RGDfK) groups and three tris-(hydroxypyridinone) groups, each attached through a tripodal scaffold to a central phenyl group via thiourea linkages. Similarly, the compound SCN-HP$_3$ (Chart 1), synthesized as previously described,[18] was reacted with (i) RGD$_3$ and (ii) c(RGDfK) under the same microwave conditions. This provided the derivatives HP$_3$-RGD$_3$ and HP$_3$-RGD (Chart 1) which are trimeric and monomeric c(RGDfK) homologues of HP$_9$-RGD$_3$, the former two conjugates containing only a single tris(hydroxypyridinone) ligand for coordination of a single metal ion. These conjugates were also purified using RP-HPLC and isolated in ≥95% purity (as previously reported for HP$_3$-RGD[18]).

Reaction of Hydroxypyridinone Derivatives with ^{68}Ga^{3+}/^{nat}Ga^{3+}. Solutions of HP$_9$-RGD$_3$, HP$_3$-RGD$_3$, and HP$_3$-RGD were added to an excess of ^{nat}Ga(NO$_3$)$_3$. For each of these solutions, the reverse phase LCMS total ion chromatogram revealed Ga^{3+} complexation of the hydroxypyridinone conjugates (Figure 1). As predicted, the conjugate HP$_9$-RGD$_3$ that contains nine hydroxypyridinone groups (three hexadentate tris(hydroxypyridinone) groups) coordinated three Ga^{3+} metal ions, whereas the conjugates HP$_3$-RGD$_3$ and HP$_3$-RGD, each possessing only a single tris-(hydroxypyridinone) chelator, were bound to only a single Ga^{3+} ion. In each case, the most intense set of peaks in the mass

DOI: 10.1021/acs.bioconjchem.6b00621
Bioconjugate Chem. 2017, 28, 481−495

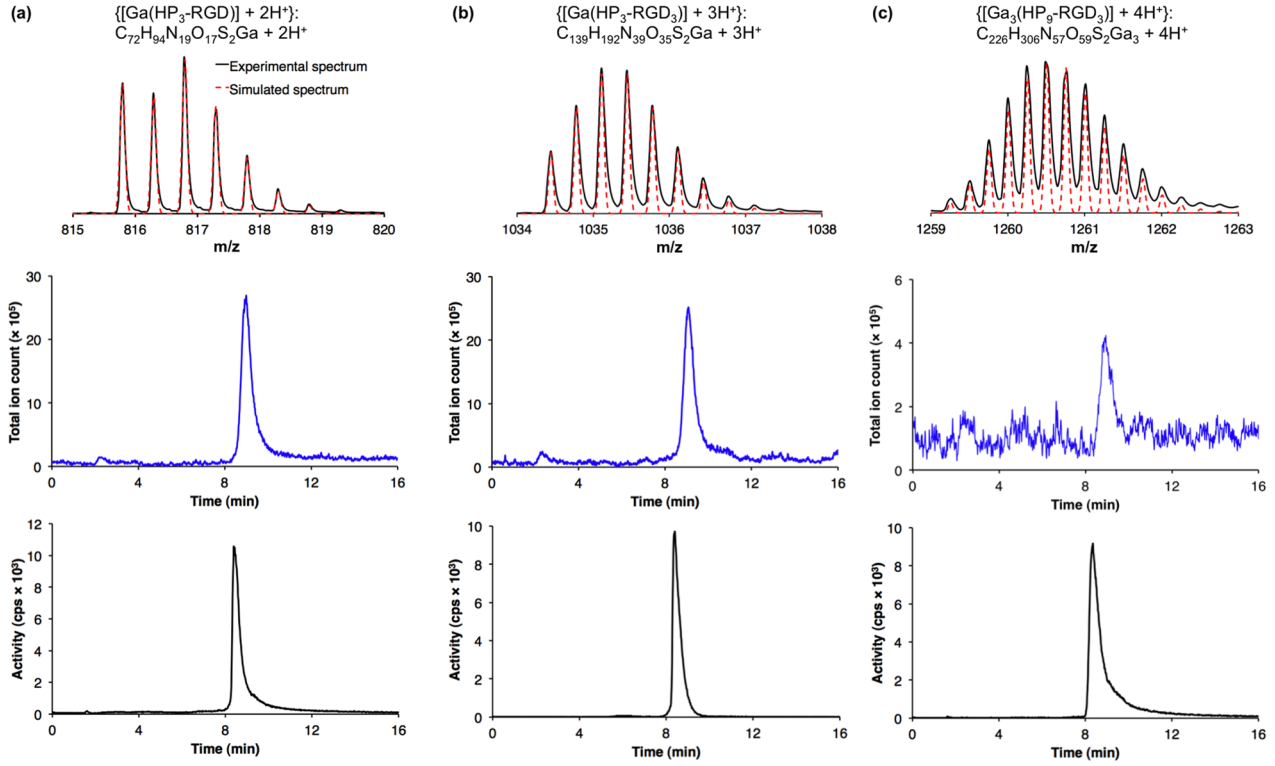

Figure 1. Radio-HPLC chromatogram of ^{68}Ga-labeled peptide conjugates (bottom, black traces), and total ion count LCMS chromatograms of ^{nat}Ga-complexed peptide conjugates acquired using the same mobile phase conditions (middle, blue traces); mass spectral signals associated with each LCMS chromatographic signal (top, black—experimental signal, red—calculated signal): (a) [Ga(HP$_3$-RGD)], (b) [Ga(HP$_3$-RGD$_3$)], (c) [Ga$_3$(HP$_9$-RGD$_3$)].

Table 1. Observed and Calculated *m/z* Values for Mass Spectral Signals of [Ga(HP$_3$-RGD)], [Ga(HP$_3$-RGD$_3$)], and [Ga$_3$(HP$_9$-RGD$_3$)], HPLC Retention Times of $^{nat/68}$Ga Labeled Conjugates, and Log *D* values of ^{68}Ga Labeled Conjugates

compound	stoichiometry of observed MS signal	observed (and calculated) *m/z* (monoisotopic)	LCMS retention time (min)	radio-HPLC retention time (min)	log $D_{OCT/PBS}$ (±SD)
[$^{nat/68}$Ga(HP$_3$-RGD)]	$C_{72}H_{94}N_{19}O_{17}S_2Ga$ + 2H$^+$	815.80 (815.80)	9.00	8.38	−2.62 ± 0.05
[$^{nat/68}$Ga(HP$_3$-RGD$_3$)]	$C_{139}H_{192}N_{39}O_{25}S_2Ga$ + 3H$^+$	1034.45 (1034.45)	9.05	8.37	−2.23 ± 0.05
[^{nat}Ga$_3$/^{68}Ga(HP$_9$-RGD$_3$)]	$C_{226}H_{306}N_{57}O_{59}S_2Ga_3$ + 4H$^+$	1259.26 (1259.25)	8.88	8.32	−2.05 ± 0.19

spectrum (Figure 1) corresponding to this chromatographic signal matched the stoichiometry of the complexes of formulas listed in Table 1.

Solutions of ^{68}Ga^{3+} produced from a ^{68}Ge/^{68}Ga generator (80−120 MBq mL^{-1}, 0.1 M HCl aqueous solution, 1 mL) were added to HP$_9$-RGD$_3$, HP$_3$-RGD$_3$, and HP$_3$-RGD and immediately adjusted to pH 6 by addition of ammonium acetate solution (1 M, 300 μL). As previously described,[18,19] these radiolabeling reactions proceeded rapidly at room temperature in less than 5 min, providing radiolabeled conjugates in >98% radiochemical yield. These mixtures were analyzed using the same HPLC conditions as those employed for the above LCMS studies. Each reaction solution gave rise to only a single signal in the radiochromatogram, each with a similar retention time to corresponding LCMS chromatogram signals (Figure 1, Table 1). Under these conditions, the maximum occupancy of bioconjugate molecules by ^{68}Ga^{3+} was low—for HP$_9$-RGD$_3$, maximum occupancy was <0.03%, and for HP$_3$-RGD$_3$ or HP$_3$-RGD, maximum occupancy was <0.01%.

To discern whether [Ga(HP$_9$-RGD$_3$)] could be chromatographically distinguished from [Ga$_2$(HP$_9$-RGD$_3$)] and [Ga$_3$(HP$_9$-RGD3)], solutions of HP$_9$-RGD$_3$ were added to aqueous solutions containing 1, 2, or 3 equiv of Ga^{3+}, and the samples were analyzed by reverse phase LCMS coupled to a UV detector (Figure 2) using a less steep solvent gradient than that employed above. [Note: To avoid confusion over the oxidation state of the metal and the pH being monitored, we adopt normal convention in showing peptides as neutral or uncharged ligands either alone or in metal complexes, even though Arg/R side chains are protonated in water at pH < 9, and Asp/D side chains are deprotonated at pH > 5. Additionally, we have elected not to indicate the protonation state of HP groups in our nomenclature, even though at pH < 4.5 in water, HP groups are protonated bearing a single positive charge, and >8 HP groups are deprotonated bearing a single negative charge. At pH 5−7.5 in water, HP groups are neutral. Upon coordination to a metal ion, each bidentate HP group is deprotonated, formally bearing a single negative charge. Thus, HP$_3$ and HP$_9$ groups and trivalent metal complexes thereof are uncharged at pH 5−7.5 in aqueous solutions.] When an analytical HPLC column was utilized for LCMS analysis, the UV chromatogram of non-Ga-treated HP$_9$-RGD$_3$ revealed at least three species (Figure 2b). The mass spectrum indicated that these species corresponded to [Al(HP$_9$-RGD$_3$)], [AlFe-(HP$_9$-RGD$_3$)], [Fe(HP$_9$-RGD$_3$)], and [Fe$_2$(HP$_9$-RGD$_3$)] (Figure 2b). It is likely that the metal ions that gave rise to

DOI: 10.1021/acs.bioconjchem.6b00621
Bioconjugate Chem. 2017, 28, 481−495

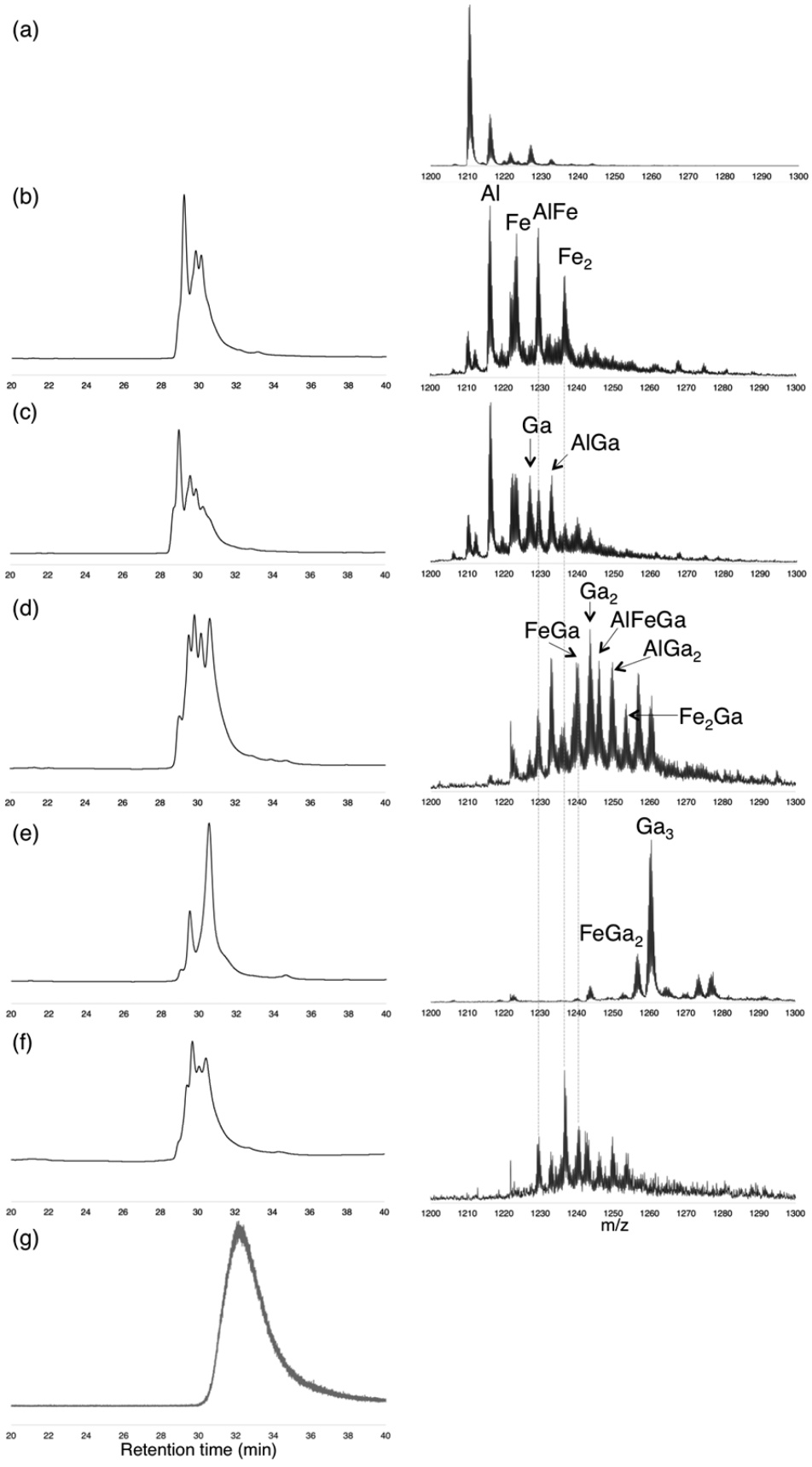

Figure 2. (a) Mass spectrum (right) of HP_9-RGD_3 acquired immediately after preparative HPLC purification (without analytical HPLC separation). Analytical HPLC UV chromatograms (left) and mass spectra (right) of solutions of HP_9-RGD_3 with (b) no added Ga^{3+}, (c) 1 equiv of Ga^{3+}, (d) 2 equiv of Ga^{3+}, (e) 3 equiv of Ga^{3+}, (f) ^{68}Ga generator eluate; (g) HPLC radiochromatogram (left) of [$^{68}Ga(HP_9$-$RGD_3)$]. Charge of mass spectral ions (z) = 4+.

DOI: 10.1021/acs.bioconjchem.6b00621
Bioconjugate Chem. 2017, 28, 481−495

these complexes came from storage vials and/or parts of the LCMS instrumentation, including the analytical reverse phase C18 column. Notably, samples of HP_9-RGD_3 isolated immediately after preparative HPLC that were not passed through an analytical HPLC column, nor lyophilized and stored for extended periods of time, contained fewer metal complex species, as measured by mass spectrometry (Figure 2a), although the [Al(HP_9-RGD_3)] complex was still prominent.

In solutions containing a single equivalent of Ga^{3+}, the major Ga-containing species corresponded to [Ga(HP_9-RGD_3)] and [AlGa(HP_9-RGD_3)], and the corresponding UV chromatograms indicated the presence of multiple species (Figure 2c). In solutions containing 2 equiv of Ga^{3+}, several Ga-containing species could be detected including [AlGa(HP_9-RGD_3)], [FeGa(HP_9-RGD_3)], [Ga_2(HP_9-RGD_3)], [AlFeGa(HP_9-RGD_3)], [$AlGa_2$(HP_9-RGD_3)], and [Fe_2Ga(HP_9-RGD_3)] (Figure 2d). Similarly, the corresponding UV chromatogram indicated the presence of multiple species. Lastly, when 3 equiv of Ga^{3+} were added to HP_9-RGD_3, only two Ga-containing species were observed: [$FeGa_2$(HP_9-RGD_3)] and [Ga_3(HP_9-RGD_3)] (Figure 2e). Only two significant signals were discernible in the UV chromatogram.

The same "slow" LCMS gradient coupled to UV detection was used to analyze a sample nominally described here as [^{68}Ga(HP_9-RGD_3)] (Figure 2f,g). The concentration of ^{68}Ga was too low to allow detection of ^{68}Ga-containing species using the mass spectrometer available in our laboratory. The species of lowest molecular weight most closely matched stoichiometries of [AlFe(HP_9-RGD_3)], [Fe_2(HP_9-RGD_3)], and [FeGa(HP_9-RGD_3)]. Unlike samples of HP_9-RGD_3, neither [Al(HP_9-RGD_3)] nor [Fe(HP_9-RGD_3)] was detected. Generator eluate is known to contain significant amounts of Fe^{3+},[49] and it is likely that HP_9-RGD_3 complexes this during the radiolabeling reaction. Indeed, unpublished data from our laboratory indicate that concentrations of Fe, Al, and ^{nat}Ga in generator eluate (0.1 M HCl, from an Eckert and Ziegler generator) are approximately 0.5 μM, 3 μM, and 1 μM, respectively. At these concentrations, Fe^{3+}, Al^{3+}, and $^{nat}Ga^{3+}$ will compete with $^{68}Ga^{3+}$ (present at picomolar concentrations) for ligand coordination, accounting for low percentage occupancy by $^{68}Ga^{3+}$ of all three conjugates. Most importantly, the radiolabeled species in solution, referred to as [^{68}Ga(HP_9-RGD_3)] for the purposes of simple nomenclature, most likely corresponds to [M_2^{68}Ga(HP_9-RGD_3)] or [M^{68}Ga(HP_9-RGD_3)] (M = Al, Fe, or ^{nat}Ga). Thus, in vivo studies, described herein, measure the biodistribution of ^{68}Ga-labeled HP_9-RGD_3 in which one or two tris(hydroxypyridinone) sites are occupied by nonradioactive metal ions. The resolution of the scintillation detector was lower than the resolution of the UV detector, and using the same gradient, the radiochromatogram of [^{68}Ga(HP_9-RGD_3)] gave rise to a single, very broad peak, coincident with the UV chromatogram signals.

Significantly higher amounts of $^{68}Ga^{3+}$ were utilized to assess the maximum specific activity that could be complexed quantitatively by the conjugates. In this procedure, $^{68}Ga^{3+}$ eluted from an iThemba generator was processed to preconcentrate the generator eluate and remove ^{68}Ge breakthrough.[50] The final $^{68}Ga^{3+}$ solution consisted of 700−1000 MBq $^{68}Ga^{3+}$ in H_2O/ethanol (82%/18%, with [HCl] = 0.18 M, total volume = 1 mL). The conjugates HP_9-RGD_3, HP_3-RGD_3, and HP_3-RGD were added to this solution followed by ammonium acetate and saline to obtain solutions (2.5 mL total volume) at pH 5.5−6.5 that were suitable for in vivo administration. Radiochemical yields of >97% were achieved using a minimum of 4 nmol of HP_9-RGD_3 and 12 nmol of either HP_3-RGD_3 or HP_3-RGD. Decreasing the amount of either HP_3-RGD_3 or HP_3-RGD to 4 nmol decreased the radiochemical yield (86% and 88%, respectively). Again, these reactions proceeded rapidly (<5 min) at room temperature, illustrating the utility of tris(hydroxypyridinone) chelators for applications requiring rapid, kit-based labeling. The maximum specific activity of ^{68}Ga-labeled HP_9-RGD_3 (180−240 MBq nmol^{-1}) compared with that of HP_3-RGD_3 or HP_3-RGD (60−80 MBq nmol^{-1}) was 3-fold higher. The maximum occupancy by $^{68}Ga^{3+}$ per molecule of bioconjugate was low in all cases. For HP_9-RGD_3, maximum occupancy was <0.3%, and for HP_3-RGD_3 or HP_3-RGD, maximum occupancy was <0.1%.

Hydrophilicity of ^{68}Ga-Radiolabeled Tracers, and Affinity for $\alpha_v\beta_3$ Integrin Receptor. The log $D_{OCT/PBS}$ values of the ^{68}Ga-labeled conjugates indicated that all three radiotracers possess comparable hydrophilicity (Table 1), with log D values all in the range of −2.7 to −2.0. These data are consistent with the similar reverse-phase HPLC retention times observed for all three radiotracers.

The half-maximal inhibitory concentration (IC_{50}) values of c(RGDfK), [Ga(HP_3-RGD)], [Ga(HP_3-RGD_3)], and [Ga_3(HP_9-RGD_3)] were determined using a cell-free solid-phase competitive binding assay with ^{125}I-echistatin. Binding of ^{125}I-echistatin to $\alpha_v\beta_3$ integrin was inhibited by all compounds in a concentration-dependent manner broadly indicating that [Ga(HP_3-RGD)], [Ga(HP_3-RGD_3)], and [Ga_3(HP_9-RGD_3)] retained affinity for $\alpha_v\beta_3$ integrin (Table 2, Figure S1). The IC_{50} value of [Ga(HP_3-RGD)] (46 ± 16 nM) was comparable to that of c(RGDfK) (28 ± 8 nM), demonstrating that conjugation did not markedly affect affinity for the $\alpha_v\beta_3$ integrin receptor. However, the IC_{50} values of [Ga(HP_3-RGD_3)] (73 ± 22 nM) and [Ga_3(HP_9-RGD_3)] (79 ± 28 nM) were higher than those of c(RGDfK) and [Ga(HP_3-RGD)], suggesting that, in this series of compounds, the presence of three copies of c(RGDfK) peptide on a single molecule did not impart higher affinity toward $\alpha_v\beta_3$ integrin compared to the monomeric THP derivative. This was surprising given that it has been reported that other dimeric,[22,23] trimeric,[27] and multimeric[51] RGD peptides demonstrate higher affinities for $\alpha_v\beta_3$ integrin than their monomeric homologues. The addition of the dendritic HP_9 chelator did not affect affinity of RGD_3 for $\alpha_v\beta_3$ integrin—IC_{50} values of [Ga_3(HP_9-RGD_3)] and [Ga_3(HP_3-RGD_3)] were very similar.

Table 2. IC_{50} Values for c(RGDfK), [Ga(HP_3-RGD)], [Ga(HP_3-RGD_3)], and [Ga_3(HP_9-RGD_3)], Determined Using a Solid-Phase Competitive Binding Assay with ^{125}I-Echistatin

compound	IC_{50} (nM) (±standard error)	95% confidence interval (nM)
c(RGDfK)	28 ± 8	12−45
[Ga(HP_3-RGD)]	46 ± 16	13−79
[Ga(HP_3-RGD_3)]	73 ± 22	30−116
[Ga_3(HP_9-RGD_3)]	79 ± 28	23−134

Biodistribution of ^{68}Ga-Labeled RGD Conjugates. The biodistribution of [^{68}Ga(HP_9-RGD_3)], [^{68}Ga(HP_3-RGD_3)], and [^{68}Ga(HP_3-RGD)] was assessed in Balb/c nu/nu mice bearing $\alpha_v\beta_3$ integrin-positive glioblastoma U87MG tumors (n = 3).

DOI: 10.1021/acs.bioconjchem.6b00621
Bioconjugate Chem. 2017, 28, 481−495

Each animal was administered 18−33 MBq of ^{68}Ga-labeled tracer and PET scanned at either 1 or 2 h post-injection (PI) for 10 min, followed immediately by euthanasia and organ harvesting for ex vivo radioactivity counting. To assess specificity of each radiotracer, a separate group of animals was coadministered c(RGDfK) (0.4 mg per animal) with the tracer, followed by scanning, euthanasia, and ex vivo organ counting 1 h PI.

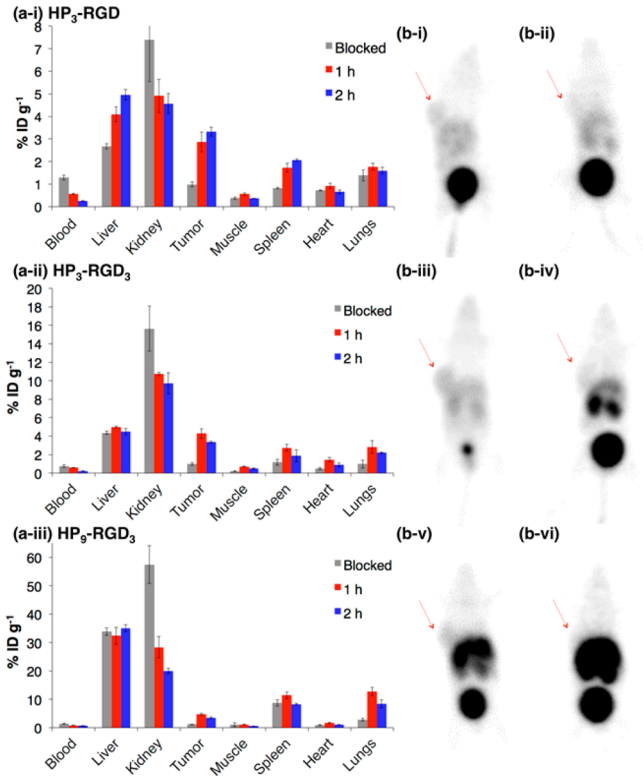

Figure 3. (a) Ex vivo biodistribution of mice bearing $\alpha_v\beta_3$ integrin-positive U87MG tumors administered (a-i) [^{68}Ga(HP$_3$-RGD)], (a-ii) [^{68}Ga(HP$_3$-RGD$_3$)], and (a-iii) [^{68}Ga(HP$_9$-RGD$_3$)], 1 and 2 h PI, and 1 h PI of coadministered c(RGDfK) (blocked); n = 3. Error bars correspond to standard error of the mean. (b) Representative PET maximum intensity projections of Balb/c nu/nu mice bearing a U87MG tumor on right flanks at 1 h PI of (b-i) [^{68}Ga(HP$_3$-RGD)], (b-ii) [^{68}Ga(HP$_3$-RGD)] + c(RGDfK), (b-iii) [^{68}Ga(HP$_3$-RGD$_3$)], (b-iv) [^{68}Ga(HP$_3$-RGD$_3$)] + c(RGDfK), (b-v) [^{68}Ga(HP$_9$-RGD$_3$)], and (b-vi) [^{68}Ga(HP$_9$-RGD$_3$)] + c(RGDfK). Red arrow indicates position of tumors on animals.

Ex vivo biodistribution data (Figures 3 and S2, and Tables 3, 4, and S1) demonstrated that tumor uptake of dendritic [^{68}Ga(HP$_9$-RGD$_3$)] was 1.75-fold higher than that of monomeric [^{68}Ga(HP$_3$-RGD)] at 1 h PI. Tumor uptake of trimeric [^{68}Ga(HP$_3$-RGD$_3$)] was 1.49-fold higher than that of [^{68}Ga(HP$_3$-RGD)]. Tumor uptake of [^{68}Ga(HP$_9$-RGD$_3$)] was higher than that of [^{68}Ga(HP$_3$-RGD$_3$)], but this was not statistically significant. By 2 h PI, there were no differences in normalized tumor uptake between the three tracers.

Table 4. Differences in Tumor Uptake of ^{68}Ga-Tracers 1 h PI, as Measured by Ex Vivo Biodistribution

comparison	mean difference 1 h PI (95% CI), %ID g^{-1}	p value
[^{68}Ga(HP$_3$-RGD)] and [^{68}Ga(HP$_3$-RGD$_3$)]	1.42 (−0.14−2.97)	0.065
[^{68}Ga(HP$_3$-RGD)] and [^{68}Ga(HP$_9$-RGD$_3$)]	1.83 (0.56−3.10)	0.016
[^{68}Ga(HP$_3$-RGD$_3$)] and [^{68}Ga(HP$_9$-RGD$_3$)]	0.41 (−1.04−1.86)	0.473

Animals administered [^{68}Ga(HP$_9$-RGD$_3$)] showed increased persistence of activity in blood, and increased liver, spleen, muscle, and lung accumulation compared to animals administered either [^{68}Ga(HP$_3$-RGD$_3$)] or [^{68}Ga(HP$_3$-RGD)] at both 1 and 2 h PI (Figure 3, Table S1). At both 1 and 2 h PI, the concentration of kidney activity for animals administered [^{68}Ga(HP$_9$-RGD$_3$)] (1 h PI, 28.32 ± 3.76%ID g^{-1}) was considerably higher than that of animals administered [^{68}Ga-(HP$_3$-RGD$_3$)] (1 h PI, 10.73 ± 0.18%ID g^{-1}), which in turn was higher than that of animals administered [^{68}Ga(HP$_3$-RGD)] (1 h PI, 4.91 ± 0.74%ID g^{-1}).

Additionally, ex vivo biodistribution data (Figures 3 and S2, Table 3) for all three tracers demonstrated that tumor uptake was target-specific at 1 h PI, with significantly lower tumor uptake for animals coadministered c(RGDfK) ("blocked" groups). In the blocked groups for all three tracers, uptake in lungs, heart, spleen, and muscle was generally lower than that observed in "nonblocked" groups. This is consistent with previous reports of receptor-mediated uptake of $\alpha_v\beta_3$ integrin targeted radiotracers,[18,22,25,27] and with the expression of $\alpha_v\beta_3$ integrin at low levels in normal vasculature tissue.[52,53] For all three tracers, radioactivity concentration in the kidneys was higher for the blocked groups than for the nonblocked groups. Similar patterns have previously been described for RGD peptide conjugates,[11] and have been attributed to slower kidney filtration rates in the presence of larger amounts of peptide.

PET imaging data for all three tracers was consistent with ex vivo biodistribution data. In PET scans of all three radiotracers acquired 1 h PI, tumors could be delineated, whereas in PET scans of animals coadministered c(RGDfK), tumors could not be delineated (Figure 3). Concentration of radioactivity in kidneys and livers for animals administered [^{68}Ga(HP$_9$-RGD$_3$)] was significantly higher than that of animals administered either [^{68}Ga(HP$_3$-RGD$_3$)] or [^{68}Ga(HP$_3$-RGD)].

Thus, although tumor uptake of dendritic [^{68}Ga(HP$_9$-RGD$_3$)] was higher at 1 h PI than that of either [^{68}Ga(HP$_3$-RGD$_3$)] or [^{68}Ga(HP$_3$-RGD)], high nontarget organ uptake of [^{68}Ga(HP$_9$-RGD$_3$)] rendered tumor to nontarget organ ratios significantly lower than that of either [^{68}Ga(HP$_3$-RGD$_3$)] or

Table 3. $\alpha_v\beta_3$ Integrin-Positive U87MG Tumor Uptake as Measured by Ex Vivo Biodistribution, 1 h PI, and 1 h PI of Coadministered c(RGDfK) (Blocked); n = 3

compound	1 h PI, %ID g^{-1} (±SEM)	with block, 1 h PI, %ID g^{-1} (±SEM)	mean difference (95% CI), %ID g^{-1}	p value
[^{68}Ga(HP$_3$-RGD)]	2.86 ± 0.43	0.99 ± 0.12	1.88 (0.86−2.90)	0.0069
[^{68}Ga(HP$_3$-RGD$_3$)]	4.28 ± 0.53	0.98 ± 0.14	3.29 (2.04−4.54)	0.0019
[^{68}Ga(HP$_9$-RGD$_3$)]	4.69 ± 0.35	1.17 ± 0.11	3.52 (2.68−4.37)	0.0003

DOI: 10.1021/acs.bioconjchem.6b00621
Bioconjugate Chem. 2017, 28, 481−495

[^{68}Ga(HP$_3$-RGD)] at 1 h PI. Contrast between tumor and nontarget organs was best achieved with [^{68}Ga(HP$_3$-RGD$_3$)] (Figure S3); therefore, further imaging studies assessing $\alpha_v\beta_3$ integrin expression in a mouse model of rheumatoid arthritis utilized this tracer.

Imaging Arthritis with [^{68}Ga(HP$_3$-RGD$_3$)]. To demonstrate the broad utility of tris(hydroxypyridinone) conjugates for molecular imaging of $\alpha_v\beta_3$ integrin receptor expression, [^{68}Ga(HP$_3$-RGD$_3$)] was used to image synovial inflammation in mice with induced rheumatoid arthritis. The $\alpha_v\beta_3$ integrin receptor is associated with cell types that are involved in rheumatoid arthritis at synovial joints, including bone resorbing osteoclasts, activated macrophages, and angiogenic endothelial cells.[53,54] Previous studies have demonstrated that radiolabeled RGD peptides target arthritic tissue[55−57] as well as osteoclasts.[58]

In these experiments, [^{68}Ga(HP$_3$-RGD$_3$)] (8−13 MBq) was administered to healthy mice (C57Bl/6 male 6−8 week mice), and mice with induced mild and severe rheumatoid arthritis.[59,60] A separate group of animals with severe rheumatoid arthritis was administered both [^{68}Ga(HP$_3$-RGD$_3$)] and an excess of c(RGDfK) to assess specificity of in vivo targeted accumulation. Prior to induction of arthritis and administration of radiotracer, the diameters of wrist and ankle joints of all animals were measured using calipers to score the severity of arthritis. At 1 h PI of radiotracer, animals were euthanized by CO_2 asphyxiation followed by PET scanning and organ collection for ex vivo biodistribution.

For all animals, radioactivity concentrations in nontarget tissues and organs, as determined by ex vivo biodistribution data (Figure S4), were consistent with results obtained from animals bearing U87MG tumors administered the same radiotracer. Blockade studies with c(RGDfK) in rheumatoid arthritis animals also indicated that some localization of [^{68}Ga(HP$_3$-RGD$_3$)] in all harvested organs except the kidneys was likely to be receptor-mediated (Table S2).

The ex vivo biodistribution data demonstrated that the amount of radioactivity in severely arthritic joints (increase in wrist and ankle diameter >0.5 mm) was higher than that in joints of healthy animals, or in joints of animals with mild arthritis (increase in wrist and ankle diameter <0.5 mm). In this analysis, joints were grouped according to their type (wrist or ankle) and the increase in swelling (caliper joint measurements) from point of disease induction to the point of imaging (8 days). Total %ID is reported rather than %ID g^{-1}, because of the large experimental error associated with dissecting and measuring the mass of mouse joint tissue. In severely arthritic joints, there was significantly higher radioactivity accumulation than in joints that were not classified as severely arthritic (including healthy animals and animals induced with mild arthritis) (Figure 4, Table 5). On the basis of %ID, severely arthritic joints could be differentiated from healthy joints, or joints that did not exhibit severe inflammation. Furthermore, blockade studies in severely arthritic animals demonstrated that uptake of [^{68}Ga(HP$_3$-RGD$_3$)] in inflamed arthritic joints was receptor-mediated (Figure 4, Table 5). Joint uptake in severely arthritic animals coadministered [^{68}Ga(HP$_3$-RGD$_3$)] and c(RGDfK) peptide was significantly lower than that of severely arthritic animals administered solely [^{68}Ga(HP$_3$-RGD$_3$)].

When animals' joints were grouped according to extent of disease (classified according to whether animals were induced with mild or severe arthritis rather than increase in joint swelling), there were no statistically significant differences in joint uptake between healthy mice and mice with mild arthritis. There were statistically significant differences between healthy mice and mice with severe arthritis, and between mice with mild arthritis and those with severe arthritis (Figure S5, Table S3).

PET scans were consistent with biodistribution data (Figure 5). In PET images acquired 1 h PI, severely arthritic joints could be distinguished from joints that were not inflamed, both

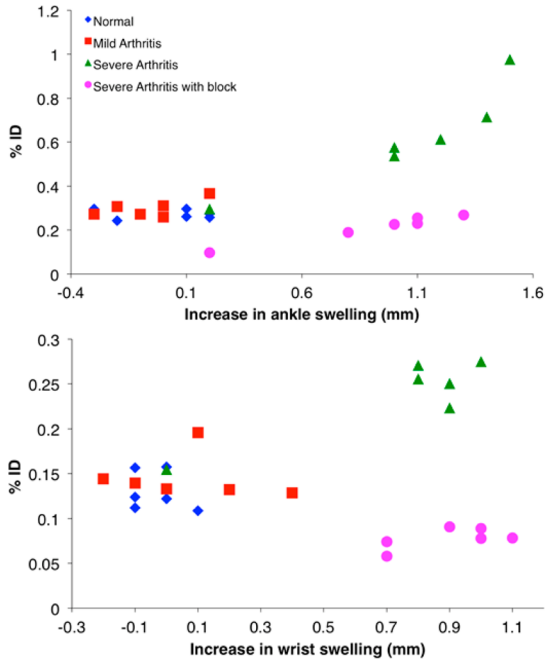

Figure 4. Ex vivo biodistribution of arthritic joints of healthy mice (blue), mice with induced mild rheumatoid arthritis (red) and mice with induced severe rheumatoid arthritis (green), administered [^{68}Ga(HP$_3$-RGD$_3$)] (8−13 MBq). A blockade study was also undertaken in mice with induced severe rheumatoid arthritis, in which [^{68}Ga(HP$_3$-RGD$_3$)] was coadministered with cRGDfK (pink). Top: %ID in feet/ankle joints; bottom: %ID in hand/wrist joints. Increase in swelling of joints was measured as the increase from the point of induction of arthritis to PET scanning/biodistribution studies (8 days).

Table 5. Ex Vivo Biodistribution of Joints of Mice Administered [^{68}Ga(HP$_3$-RGD$_3$)]

group	%ID 1 h PI (±SEM)	mean difference (95% CI) compared to severely arthritic joints, %ID	p value
	Wrists		
severely arthritic (>0.5 mm increase)	0.26 ± 0.02	-	-
severely arthritic with block	0.08 ± 0.01	0.18 (0.16−0.20)	<0.0001
healthy or mildly arthritic (<0.5 mm increase)	0.14 ± 0.02	0.12 (0.09−0.14)	<0.0001
	Ankles		
severely arthritic (>0.5 mm increase)	0.68 ± 0.18	-	-
severely arthritic with block	0.24 ± 0.02	0.44 (0.27−0.63)	0.0005
healthy or mildly arthritic (<0.5 mm increase)	0.29 ± 0.03	0.39 (0.30−0.50)	<0.0001

DOI: 10.1021/acs.bioconjchem.6b00621
Bioconjugate Chem. 2017, 28, 481−495

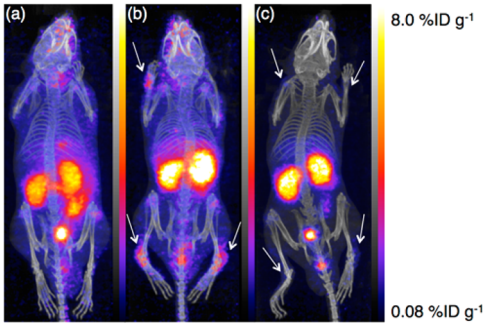

Figure 5. PET/CT maximum intensity projections of mice administered [^{68}Ga(HP$_3$-RGD$_3$)] (8−13 MBq) 1 h PI (all PET images scaled from 0.08 to 8.0%ID g^{-1}): (a) a healthy C57Bl/6 mouse; (b) a C57Bl/6 mouse with severe rheumatoid arthritis; (c) a C57Bl/6 mouse with severe rheumatoid arthritis coadministered c(RGDfK). Arrows indicate joints with an increase in swelling >0.5 mm.

between different animals (Figure 5a vs b) and within the same animal (Figure 5b). For example, within one animal with severe arthritis, the left wrist was severely inflamed (a 1 mm increase in swelling from the point of disease induction) but the right demonstrated no swelling throughout the disease induction period. In the PET/CT scan, higher radiotracer uptake was discernible in the left wrist compared to the right wrist (Figure 5b), consistent with ex vivo biodistribution data.

■ DISCUSSION AND CONCLUDING REMARKS

Multimeric receptor-targeted radiolabeled agents, in which each molecule contains either multiple copies of each targeting peptide, or multiple copies of a multidentate chelator,[42] can deliver increased radioactive payloads to target tissue relative to monomeric homologues. Dimeric,[25,61−63] trimeric,[8,27] tetrameric,[64,65] and octameric[66] RGD conjugates radiolabeled with metallic PET isotopes have demonstrated efficacious $\alpha_v\beta_3$ integrin targeting in vivo. Herein, we have described the first radiolabeled molecular compound that integrates multiple copies of a chelator and multiple copies of peptide, in this case, $\alpha_v\beta_3$ integrin-targeted c(RGDfK). In contrast to previous work on multimeric RGD peptide conjugates, the new dendritic system possesses tris(hydroxypyridinone) chelators that coordinate ^{68}Ga^{3+} quantitatively at ambient temperature, near neutral pH, and micromolar concentrations of conjugate, allowing for rapid, one-step labeling.

Synthesis of HP$_9$-RGD$_3$, which consists of a bifunctional enneakis(hydroxypyridinone) ligand attached to a trimeric peptide targeting $\alpha_v\beta_3$ integrin receptors, enabled assessment of whether dendritic chelator systems could enhance specific activity in radiolabeled molecular imaging agents. Incorporation of multiple hexadentate tris(hydroxypyridinone) groups into a single construct, HP$_9$-RGD$_3$, increased specific activity relative to HP$_3$ derivatives. At concentrations of ∼1.6 μM, near-quantitative radiochemical yields (>97%) were achieved for HP$_9$-RGD$_3$, whereas for HP$_3$-RGD and HP$_3$-RGD$_3$, concentrations of 5 μM were required to achieve the same radiochemical yields. The maximum specific activity of ^{68}Ga-labeled HP$_9$-RGD$_3$ (180−240 MBq nmol^{-1}) was 3-fold higher when compared with that of HP$_3$-RGD$_3$ or HP$_3$-RGD (60−80 MBq nmol^{-1}).

Analytical HPLC using a UV detector (interfaced with a mass spectrometer and a gamma scintillation detector) could distinguish numerous signals arising from a sample of [^{68}Ga(HP$_9$-RGD$_3$)]. For the same sample, line widths of signals in the radiochromatogram and the TIC chromatograms were much broader, and could not be precisely correlated with individual signals in the UV chromatogram. Mass spectral analysis indicated that all tris(hydroxypyridinone) sites in [^{68}Ga(HP$_9$-RGD$_3$)] were likely occupied by trivalent metal ions. Hexadentate THP-Ac has a very high affinity for Fe^{3+}, with log K_1 = 32.52 and pFe^{3+} = 28.47 at pH 7.4 ([Fe^{3+}] = 10^{-6} M, [Ligand] = 10^{-5} M).[17] Dendritic derivatives have similar affinities.[17] While affinities of 3-hydroxy-4-pyridinones for Al^{3+} are normally several orders of magnitude lower than for Fe^{3+}, they are still high—for example, for a series of tripodal tris(hydroxypyridinones), pAl^{3+} consistently measured 21−22 at pH 7.4.[16] It is unsurprising that in ^{68}Ga-labeled HP$_9$-RGD$_3$, tris(hydroxypyridinone) sites unoccupied by ^{68}Ga^{3+} complex adventitious Fe^{3+}, Al^{3+}, and ^{nat}Ga^{3+}.

It was hypothesized that the higher specific activity and the trimeric peptide nature of [^{68}Ga(HP$_9$-RGD$_3$)] might result in targeted tumor delivery of a comparatively higher radioactive payload per molecule of receptor-bound bioconjugate compared to [^{68}Ga(HP$_3$-RGD$_3$)] and [^{68}Ga(HP$_3$-RGD)].

Despite the lower IC$_{50}$ value of the monomeric [^{68}Ga(HP$_3$-RGD)] species, its in vivo normalized tumor accumulation (as measured by ex vivo biodistribution) was lower than that of trimeric [^{68}Ga(HP$_3$-RGD$_3$)] and dendritic [^{68}Ga(HP$_9$-RGD$_3$)] at 1 h PI (Figure 3). The radiotracers' pharmacokinetics as well as $\alpha_v\beta_3$ integrin affinities are likely to be important in influencing their relative tumor uptake. It is possible that in vivo, blood clearance of [^{68}Ga(HP$_3$-RGD)] was faster than that of [^{68}Ga(HP$_3$-RGD$_3$)] and [^{68}Ga(HP$_9$-RGD$_3$)] at early time points (before 1 h PI), resulting in higher tumor bioavailability and thus higher uptake of [^{68}Ga(HP$_3$-RGD$_3$)] and [^{68}Ga(HP$_9$-RGD$_3$)] 1 h PI. Additionally, for HP$_9$-RGD$_3$, it is likely that there was comparatively lower occupancy of target $\alpha_v\beta_3$ integrin in vivo by unlabeled conjugate. Comparable amounts of radioactivity were administered to each mouse for the three different radiotracers, but in the case of HP$_9$-RGD$_3$, ∼0.15 nmol of conjugate was administered to each animal, compared to ∼0.5 nmol for HP$_3$-RGD$_3$ and HP$_3$-RGD.

There was an increase in radioactivity concentration in tumors at 1 h PI for [^{68}Ga(HP$_9$-RGD$_3$)] compared to [^{68}Ga(HP$_3$-RGD$_3$)] (mean difference = 0.41%ID g^{-1}), and for [^{68}Ga(HP$_3$-RGD$_3$)] compared to [^{68}Ga(HP$_3$-RGD)] (mean difference = 1.42%ID g^{-1}) (Tables 3, 4). There was a statistically significant increase (mean difference = 1.83%ID g^{-1}) in tumor accumulation at 1 h PI for [^{68}Ga(HP$_9$-RGD$_3$)] compared to [^{68}Ga(HP$_3$-RGD)]. Thus, the *combination* of increased specific activity and a multimeric effect could be responsible for this increase in radioactivity concentration in tumors of animals administered the dendritic radiotracer. Such an observation lends credence to the hypothesis that dendritic radiotracers that incorporate multiple chelating groups and copies of targeting peptides can increase radioactive payload at tissue, relative to monomeric homologues. The higher mean difference in tumor uptake between [^{68}Ga(HP$_3$-RGD$_3$)] and [^{68}Ga(HP$_3$-RGD)], compared to [^{68}Ga(HP$_9$-RGD$_3$)] and [^{68}Ga(HP$_3$-RGD$_3$)], suggests that the presence of a multimeric peptide is the more significant of the two factors in enhancing tumor uptake.

The distance between c(RGDfK) groups in HP$_3$-RGD$_3$ and HP$_9$-RGD$_3$ is not sufficient to allow simultaneous binding to two or more $\alpha_v\beta_3$ integrin receptors. It is possible that

DOI: 10.1021/acs.bioconjchem.6b00621
Bioconjugate Chem. 2017, 28, 481−495

increasing this distance to allow simultaneous binding could result in higher uptake and retention in tissue that over-expresses $\alpha_v\beta_3$ integrin receptors.[62,63]

We have previously demonstrated that THP peptide conjugates can rapidly and quantitatively complex $^{68}Ga^{3+}$ at near-neutral pH, ambient temperature, and low chelator concentrations, and that the resulting radiotracers can delineate tumor tissue in vivo.[18,19] [^{68}Ga(HP$_3$-RGD$_3$)], prepared using simple radiolabeling procedures, can image synovial inflammation in mice with induced rheumatoid arthritis, distinguishing severely arthritic joints from disease-free joints. Few data are available on $\alpha_v\beta_3$ integrin targeted radiotracers for rheumatoid arthritis,[55,56] and the mouse models employed in previously published studies differ from the model utilized here. However, we note that [^{68}Ga(HP$_3$-RGD$_3$)] uptake in severely arthritic synovial joints of mice in a serum transfer-induced arthritis model (0.26 ± 0.02%ID in wrists and 0.68 ± 0.18%ID in ankles 1 h PI) is comparable to ^{111}In-DOTA-E(RGDfK)$_2$ uptake in mice in a collagen-induced arthritis model (0.2 ± 0.1%ID in arthritic joints at 1 h PI).[55]

Rheumatoid arthritis is currently diagnosed using information from physical examination (signs and symptoms), blood tests, X-rays, and MRI. Ideally, it is diagnosed early so that treatment that slows or halts disease progression can begin. Current early diagnostic methods detect anatomical changes in patients' joints and so arthritic sites in patients that are not symptomatic or visually identifiable are missed.[67,68] PET/CT imaging of $\alpha_v\beta_3$ integrin expression using kit-based radiopharmaceuticals could provide whole-body diagnosis at early stages of disease before the manifestation of debilitating symptoms, as well as monitor patient response throughout treatment, providing greater effectiveness of treatment at early stages of disease. Such radiotracers could also be used to predict whether an individual patient will respond to a particular molecular therapeutic, based on the presence of a therapeutic receptor target. The availability of ^{68}Ga from a benchtop generator, coupled with a chelator conjugate that enables one-step, kit-based syntheses, which are not readily achievable with other chelators, brings about the possibility of widely available whole body PET molecular imaging of rheumatoid arthritis without the need for a local cyclotron or automated radiosynthesis equipment.

EXPERIMENTAL SECTION

Materials and Instrumentation. Chemicals and reagents were obtained from Sigma-Aldrich (Dorset, UK) unless otherwise specified. High-performance liquid chromatography (HPLC) analysis was carried out using an Agilent 1200 LC system with in-line UV and gamma detection (Flow-Count, LabLogic). NMR spectra were acquired on either a Bruker Avance 400 or 700 spectrometer (Bruker UK Limited, Coventry, UK). Spectra were referenced to residual solvent signals. Mass spectra were recorded in the positive ion mode on an Agilent 6510 Q-TOF LC/MS mass spectrometer coupled to an Agilent 1200 LC system (Agilent, Palo Alto, CA). Data were acquired and reference mass-corrected via a dual-spray electrospray ionization source, using the factory-defined calibration procedure. Analytical reverse-phase LCMS and radio-LCMS traces were acquired using an Agilent Eclipse XDB-C18 column (4.6 × 150 mm, 5 μm). Instant thin layer chromatography strips (ITLC-SG) were obtained from Varian Medical Systems UK, Ltd. (Crawley, UK), and ITLC strips were visualized using a Raytest Rita-Star TLC scanner. Semipreparative reverse-phase HPLC was conducted using an Agilent Eclipse XDB-C18 column (9.4 × 250 mm, 5 μm) coupled to an Agilent 1200 LC system, with a 3 mL min^{-1} flow rate and UV spectroscopic detection at 220 nm. Mobile phase A contained water with 0.2% TFA and mobile phase B contained acetonitrile with 0.2% TFA. All methods started with 100% A at 0 min. For method 1, the concentration of B increased at a rate of 2% min^{-1}; for method 2, the concentration of B increased at a rate of 1% min^{-1}; and for method 3, the concentration of B increased at a rate of 0.5% min^{-1}. Analytical reverse-phase HPLC and radio-HPLC traces were acquired using two different instruments: (1) an Agilent 1200 LC system and an Agilent Zorbax Eclipse XDB-C18 column (4.6 × 150 mm, 5 μm) with a 0.25−1 mL min^{-1} flow rate and UV spectroscopic detection at either 214 or 220 nm. The radio-HPLC was coupled to a LabLogic Flow-Count detector with a sodium iodide probe (B-FC-3200). Aliquots (10−200 μL) of each radiolabeled sample were injected onto the column. Mobile phase A contained water with 0.1% TFA and mobile phase B contained acetonitrile with 0.1% TFA. For method 4, flow rate was 1 mL min^{-1}, the concentration of B increased at a rate of 5% min^{-1}, with 100% A at 0 min, and 100% B at 20 min. For method 5, flow rate was 0.25 mL min^{-1}, the concentration of B increased at a rate of 2% min^{-1}, with 100% A at 0−5 min, and 100% B at 55 min. (2) An Agilent Zorbax Eclipse XDB-C18 column (4.6 × 150 mm, 5 μm) with a 1 mL min^{-1} flow rate and UV spectroscopic detection at either 214 or 220 nm coupled to a Shimadzu HPLC consisting of a SCL-10AVP system controller, a SIL-10ADVP autoinjector, a LC-10 ATVP solvent delivery unit, a FCV-10AL control valve, a DGU-14A degasser, and a SPD-10AVP UV detector. This was coupled to a radiation detector consisting of an Ortec model 276 Photomultiplier Base with Preamplifier, Amplifier, BIAS supply, and SCA and a Bicron 1 M 11.2 Photomultiplier Tube. For method 6, the concentration of B increased at a rate of 6.67% min^{-1}, with 100% A at 0 min, and 80% B at 12 min. For initial radiolabeling and characterization studies that utilized <400 MBq, an Eckert and Ziegler ^{68}Ge/^{68}Ga generator (Berlin, Germany) was used. For biodistribution studies, and experiments that utilized >600 MBq ^{68}Ga, an iThemba Laboratories 1.8 GBq ^{68}Ge/^{68}Ga generator (IDB Holland BV, Netherlands) was used.

Tricarboxylate **1**,[17] hydroxypyridinone **2**,[69] SCN-HP$_3$, and HP$_3$-RGD were synthesized as previously described.[18] The cyclic peptide c(RGDfK) was provided by Peptide Synthetics (Fareham, UK).

Compound **4**. A solution of tricarboxylate **1** (18 mg, 40 μmol), hydroxypyridinone **2** (170 mg, 160 μmol), HATU (60 mg, 158 μmol), and diisopropylethylamine (30 μL) in DMF (2−5 mL) was heated in a microwave reactor (120 °C, 300 W, 30 min), after which the reaction solution was evaporated to dryness under reduced pressure. The residue was applied to a silica column, and eluted initially with methanol/chloroform (1:4), followed by methanol/chloroform/40% ammonium hydroxide (10:40:1). Fractions containing **3** (identified using mass spectrometry) were dried over anhydrous magnesium sulfate, filtered, and evaporated to dryness. Compound **3**: ESI-MS: m/z for $C_{195}H_{228}N_{26}O_{36}$ + $3H^+$ calc 1170.90, found 1170.90 (monoisotopic signal). Compound **3** (105 mg, 30 μmol) was added to a solution of ethanol/aqueous 5.5% hydrazine (9:1) (5 mL), and the mixture was heated in a microwave reactor (90−100 °C, 300 W, 30 min). The solution was cooled in an ice bath, and acidified with concentrated

DOI: 10.1021/acs.bioconjchem.6b00621
Bioconjugate Chem. 2017, 28, 481−495

hydrochloric acid to pH 1, filtered, and evaporated to dryness. The residue was redissolved in water/acetonitrile (2:1) and applied to a semipreparative HPLC column. Using HPLC method 1, **4** eluted with 44% B (22−25 min). Fractions containing the desired product were lyophilized. Yield = 55 mg, 40% yield (based on tricarboxylate **1**). ^{1}H NMR (CD_3OD, 400 MHz): δ 1.84 (m, 6H), 1.91 (m, 18H), 2.05 (m, 6H), 2.14 (m, 18H), 2.30 (t, J = 7.2, 6H), 2.53 (s, 27H), 2.56 (broad, 2H), 3.10 (t, J = 6.1, 2H), 3.34 (broad, 6H), 3.78 (s, 27H), 4.56 (s, 18H), 5.17 (s, 18H), 6.95 (s, 9H), 7.34 (m, 27H), 7.43 (m, 18H). ^{13}C NMR (CD_3OD, 100 MHz): δ 21.2, 31.2, 30.9, 36.5, 37.3, 37.4, 38.9, 59.0, 75.7, 117.5, 129.70, 129.71, 130.1, 137.9, 146.0, 146.4, 152.9, 170.1, 171.5, 173.2, 175.4, 175.5, quaternary carbons of tripodal scaffold obscured by CD_3OD peaks. ESI-MS: m/z for $C_{187}H_{226}N_{26}O_{34}$ + $3H^+$ calc 1127.57, found 1127.57 (monoisotopic signal).

SCN-HP$_9$. An excess of *p*-phenylene diisothiocyanate (22 mg) and diisopropylethylamine (20 μL) in DMF (0.3 mL) were added to a solution of **4** (15 mg, 4.4 μmol) in DMF (0.5−1 mL). The reaction solution was agitated, and after 5−10 min, applied to a semipreparative HPLC column. Using HPLC method 1, product **5** eluted with 48% B (24−25 min). Fractions containing compound **5** were lyophilized. Compound **5**: yield = 7 mg, 45%. ^{1}H NMR (CD_3OD, 400 MHz): δ 1.86 (m, 6H), 1.90 (m, 18H), 2.07 (m, 6H), 2.14 (m, 18H), 2.28 (t, J = 6.7, 6H), 2.46 (t, J = 6.1, 2H), 2.55 (s, 27H), 3.31 (presumed 6H, under CHD_2OD signal), 3.76 (broad, 2H), 3.80 (s, 27H), 4.58 (s, 18H), 5.18 (s, 18H), 7.00 (s, 9H), 7.14 (d, J = 9.0, 2H) 7.33 (m, 27H), 7.42 (m, 18H), 7.45 (under peak at 7.42, 2H). ESI-MS: m/z for $C_{195}H_{230}N_{28}O_{34}S_2$ + $4H^+$ calc 893.92, found 893.92 (monoisotopic signal). A solution of chilled boron trichloride in dichloromethane (5 mL, 1 M) was added to a sealed vial containing compound **5** (7 mg, 2 μmol), and the reaction was stirred at ambient temperature for 1 h. The reaction vial was then cooled in an ice bath, and methanol (5−10 mL) was added dropwise to the flask. The reaction solution was evaporated to near dryness under reduced pressure, and acetone (50 mL) was added to the residue, resulting in a flocculant white precipitate. This suspension was transferred to a 50 mL centrifuge tube, and the mixture centrifuged at 3000 rpm for 10 min. After this, the supernatant was decanted and discarded, acetone added (50 mL), the suspension agitated, and centrifuged again for 10 min. This process of washing with acetone was repeated again. Finally, the product was dissolved in water/acetonitrile (50/50), filtered, frozen, and lyophilized. The residue was applied to a semipreparative HPLC column. Using HPLC method 2, SCN-HP$_9$ eluted with 35% B (35−36 min). Fractions containing the desired product were lyophilized. Yield (trifluoroacetate salt) = 3 mg, 30−40%. ^{1}H NMR (CD_3OD, 700 MHz): δ 1.93 (t, J = 7.5, 6H), 1.96 (t, J = 7.5 18H), 2.15 (t, J = 7.5, 6H), 2.22 (t, J = 7.5, 18H), 2.33 (t, J = 6.3, 6H), 2.52 (broad, 2H), 2.57 (s, 27H), 3.35 (broad, 6H), 3.79 (broad, 2H), 3.92 (s, 27H), 4.70 (s, 18H), 6.93 (s, 9H), 7.20 (d, splitting = 8.7, 2H), 7.48 (d, splitting = 8.7, 2H). ^{13}C NMR (CD_3OD, 175 MHz): δ 19.7, 29.3, 29.7, 34.9, 35.8, 36.1, 37.9, 57.5, 112.8, 123.9, 125.7, 127.0, 135.1, 137.8, 144.0, 148.9, 161.9, 172.0, 174.3, 174.9, 175.0, 180.6, quaternary carbons of tripodal scaffold obscured by CD_3OD peaks. ESI-MS: m/z for $C_{132}H_{176}N_{28}O_{34}S_2$ + $4H^+$ calc 691.32, found 691.32 (monoisotopic signal).

RGD$_3$. A solution of DMF (5 mL) containing tricarboxylate **1** (100 mg, 220 μmol), diisopropylcarbodiimide (10 equiv), *N*-hydroxysuccinimide (4 equiv), and diisopropylethylamine (4 equiv) was stirred for 16 h, after which it was filtered, and the filtrate applied to a semipreparative HPLC column. Using HPLC method 2, product **6** eluted with 38% B (38−42 min), and fractions containing the desired compound were lyophilized. Compound **6**: isolated yield = 50 mg, 30%. ^{1}H NMR ($CDCl_3$, 400 MHz): δ 2.22 (t, J = 7.4, 6H), 2.50 (t, J = 7.0, 2H), 2.77 (s, 12H), 2.59 (t, J = 7.4, 6H), 3.92 (t, J = 7.0, 2H), 7.67 (q, splitting = 3.0, 5.5, 2H), 7.79 (q, splitting = 3.0, 5.5, 2H). ^{13}C NMR ($CDCl_3$, 100 MHz): δ 25.5, 25.8, 28.6, 34.0, 34.6, 50.0, 123.3,132.2, 134.0, 168.3, 168.5, 169.6. ESI-MS: m/z for $C_{33}H_{33}N_5O_{15}$ + H^+ calc 740.20, found 740.21. Activated triester **6** (5 mg, 7 μmol) was added to a solution of c(RGDfK) (20 mg, 24 μmol) and diisopropylethylamine (5 μL) in dimethylformamide (0.1−0.5 mL), and the solution was stirred for 10 min reaction at ambient temperature. After this time, the solution was applied to a semipreparative HPLC column. Using HPLC method 2, compound **7** eluted with 32% B (32 min). Fractions containing the desired product were lyophilized. Compound **7**: yield of trifluoroacetate salt = 7.5 mg, 42%. ESI-MS: m/z for $C_{102}H_{141}N_{29}O_{27}$ + $2H^+$ calc 1103.04, found 1103.04 (monoisotopic signal). Finally, phthalimide-protected compound **7** (15 mg) was added to a solution of ethanol/aqueous 5.5% hydrazine (9:1) (5 mL), and the mixture was heated in a microwave reactor (90−100 °C, 300 W, 30 min). The solution was then cooled in an ice bath, and acidified with concentrated hydrochloric acid to pH 1, filtered, and lyophilized. The solution was redissolved in deionized water and applied to a semipreparative HPLC column. Using HPLC method 2, RGD$_3$ eluted with 28% B (28 min). Fractions containing RGD$_3$ were lyophilized. Yield: 6 mg, 40%. ESI-MS: m/z for $C_{102}H_{141}N_{29}O_{27}$ + $4H^+$ calc 519.52, found 519.52 (monoisotopic signal); HPLC: 220 nm, RT = 7.90 min, >97% purity (HPLC method 4).

Synthesis of RGD Conjugates. RGD$_3$ was dissolved in dimethyl sulfoxide (100−300 μL) and added to a solution of either SCN-HP$_3$ or SCN-HP$_9$ in dimethyl sulfoxide (100−300 μL), and diisopropylethylamine (5−10 μL) was added. The reaction solutions were heated in a microwave (120 °C, 300 W, 30 min) and then applied to a reverse-phase HPLC column. Fractions containing the desired conjugate in sufficient purity were combined and lyophilized. Using HPLC method 3, HP$_3$-RGD$_3$ eluted with 26% solvent B (52 min) and HP$_9$-RGD$_3$ eluted with 25% solvent B (51 min). Isolated yields = 30−40%. HP$_3$-RGD$_3$: ESI-MS: m/z for $C_{139}H_{195}N_{39}O_{35}S_2$ + $5H^+$ calc 607.89, found 607.89 (monoisotopic signal); HPLC: 220 nm, RT = 8.02 min, >99% purity (HPLC method 4). HP$_9$-RGD$_3$: ESI-MS: m/z for $C_{226}H_{315}N_{57}O_{59}S_2$ + $6H^+$ calc 806.89, found 806.89 (monoisotopic signal); HPLC: 220 nm, RT = 7.77 min, >99% purity (HPLC method 4).

Complexation with $^{68}Ga^{3+}$ and $^{nat}Ga^{3+}$. Initial radiolabeling experiments utilized an Eckert and Ziegler ^{68}Ge/^{68}Ga generator. Aqueous HCl solution (0.1 M, 5 mL) was passed through the generator and the eluate was fractionated (5 × 1 mL). The second fraction (1 mL, containing 90−100 MBq ^{68}Ga) was added directly to an ethanol/water solution (50%/50%, 50−100 μL) of either HP$_3$-RGD (25 μg, 12 nmol), HP$_3$-RGD$_3$ (50 μg, 13 nmol), or HP$_9$-RGD$_3$ (25 μg, 4 nmol), immediately followed by a solution of ammonium acetate (1 M, 300 μL). This solution was immediately applied to an analytical reverse-phase C18 HPLC column. [^{68}Ga(HP$_3$-RGD)]: radiochemical yield >99% (HPLC), HPLC: RT = 8.38 min (HPLC method 4). [^{68}Ga(HP$_3$-RGD$_3$)]: radiochemical yield >99%

DOI: 10.1021/acs.bioconjchem.6b00621
Bioconjugate Chem. 2017, 28, 481−495

(HPLC), HPLC: RT = 8.37 min (HPLC method 4). [^{68}Ga(HP$_9$-RGD$_3$)]: radiochemical yield >99% (HPLC), HPLC: RT = 8.32 min (HPLC method 4). For [^{68}Ga(HP$_3$-RGD)] and [^{68}Ga(HP$_3$-RGD$_3$)], specific activity at point of synthesis = 8−9 MBq nmol^{-1} conjugate and for [^{68}Ga(HP$_9$-RGD$_3$)], specific activity = 24−27 MBq nmol^{-1}.

The nonradioactive analogues, [^{nat}Ga(HP$_3$-RGD)], [^{nat}Ga-(HP$_3$-RGD$_3$)], and [^{nat}Ga$_3$(HP$_9$-RGD$_3$)], were also prepared. An aqueous solution of Ga(NO$_3$)$_3$ (2 mg mL^{-1}, 5 μL, 30−40 nmol, excess) was added to HP$_3$-RGD (25 μg, 12 nmol), HP$_3$-RGD$_3$ (50 μg, 13 nmol), or HP$_9$-RGD$_3$ (25 μg, 4 nmol) dissolved in an ethanol/water solution (50%/50%, 50−100 μL). The solutions were applied to an analytical reverse-phase C18 HPLC column and subjected to LCMS analysis. [^{nat}Ga(HP$_3$-RGD)]: HPLC RT = 8.93 min (HPLC method 4); MS $C_{72}H_{94}N_{19}O_{17}S_2Ga$ + 2H$^+$, observed monoisotopic peak = 815.80, calculated = 815.80 (monoisotopic signal); [^{nat}Ga-(HP$_3$-RGD$_3$)]: HPLC RT = 9.05 min (HPLC method 4); MS $C_{139}H_{192}N_{39}O_{25}S_2Ga$ + 3H$^+$, observed monoisotopic peak =1034.45, calculated 1034.45 (monoisotopic signal); [^{nat}Ga$_3$(HP$_9$-RGD$_3$)]: HPLC RT = 8.88 min (HPLC method 4); MS $C_{226}H_{306}N_{57}O_{59}S_2Ga_3$ + 4H$^+$, observed monoisotopic peak = 1259.26, calculated 1259.25 (monoisotopic signal). For more detailed LCMS analysis of HP$_9$-RGD$_3$, HP$_9$-RGD$_3$ was titrated with 0, 1, 2, and 3 mol equiv of Ga(NO$_3$)$_3$, prior to analysis using LCMS (HPLC method 5).

For biodistribution with U87MG tumor bearing mice, ^{68}Ga eluate from an iThemba Lab generator was preconditioned as previously described.[50] Briefly, a cation exchange cartridge containing AG 50Wx4 resin (50 mg) was conditioned by passing through aqueous HCl solution (4 M, 1 mL) and deionized water (1 mL) sequentially. To elute the ^{68}Ge/^{68}Ga generator, aqueous HCl solution (0.4 M, 5 mL) was passed through the generator and transferred directly onto the cation exchange cartridge. The cartridge was dried with air (1 mL), washed with 0.15 M HCl in water/ethanol (20%/80%), and again dried with air (1 mL). A solution of 0.9 M HCl in water/ethanol (200 μL, 10%/90%) was used to elute ^{68}Ga (800−1000 MBq), which was diluted to a volume of 1 mL with deionized water. Lyophilized peptide conjugate (trifluoroacetate salt)—HP$_3$-RGD (25 μg, 12 nmol), HP$_3$-RGD$_3$ (50 μg, 13 nmol), or HP$_9$-RGD$_3$ (25 μg, 4 nmol)—dissolved in 20−40 μL of water/ethanol (50%/50%) was added to the solution containing ^{68}Ga, immediately followed by a solution of ammonium acetate (2 M, 400 μL) and 0.9% saline (1100 μL). An aliquot for ITLC analysis was immediately applied to an ITLC-SG plate. The ITLC-SG plate was developed using an aqueous citrate buffer (0.1 M, pH 5.5) mobile phase. [^{68}Ga(HP$_3$-RGD)], [^{68}Ga(HP$_3$-RGD$_3$)], and [^{68}Ga(HP$_9$-RGD$_3$)]: R_f < 0.1; [^{68}Ga(citrate)$_2$]$^{3-}$: R_f > 0.8. [^{68}Ga(HP$_3$-RGD)]: radiochemical yield > 95% (ITLC). HPLC (method 6): RT = 9.78 min; [^{68}Ga(HP$_3$-RGD$_3$)]: radiochemical yield > 95% (ITLC), HPLC: RT = 9.54 min; [^{68}Ga(HP$_9$-RGD$_9$)]: radiochemical yield > 95% (ITLC), HPLC: RT = 9.50 min.

Log $P_{OCT/PBS}$ Determination. A solution containing ^{68}Ga-conjugate (50 μL, synthesized using eluate from an Eckert and Ziegler generator as described above) was added to 550 μL of octanol and 500 μL of aqueous phosphate buffered saline solution. The mixture was agitated using a vortex, and the phases separated by centrifugation (1000 rpm, 2 min). Aliquots from each phase were counted for radioactivity in a gamma counter. The experiment was repeated four times.

Determination of IC_{50}. The relative affinity of [^{nat}Ga(HP$_3$-RGD)], [^{nat}Ga(HP$_3$-RGD$_3$)], [^{nat}Ga$_3$(HP$_9$-RGD$_3$)], and c-(RGDfK) for integrin $\alpha_v\beta_3$ was determined in a solid-phase competitive binding assay[18] with ^{125}I-echistatin (PerkinElmer, Boston). In brief, wells of a 96 well plate were coated with integrin $\alpha_v\beta_3$ (150 ng mL^{-1}) in coating buffer (100 μL, 25 mM Tris HCl pH 7.4, 150 mM NaCl, 1 mM CaCl$_2$, 0.5 mM MgCl$_2$, and 1 mM MnCl$_2$) overnight at 4 °C. Wells were then washed twice in binding buffer (coating buffer containing 0.1% bovine serum albumin (w/v) (BSA)) before being incubated for 2 h at room temperature with blocking buffer (coating buffer containing 1% BSA (w/v)). After a further two washes in binding buffer, ^{125}I-echistatin (0.5 kBq) and either [^{nat}Ga(HP$_3$-RGD)], [^{nat}Ga(HP$_3$-RGD$_3$)], [^{nat}Ga$_3$(HP$_9$-RGD$_3$)] or c-(RGDfK) were added simultaneously (to a total volume of 100 μL, and a conjugate/c(RGDfK) concentration of 10000 nM to 0.001 nM) for 1 h at room temperature, before being washed twice as before. Finally, the amount of activity bound to the wells via integrin $\alpha_v\beta_3$ was counted using a Wallac 1282 Compugamma Universal Gamma Counter. Measurements at each concentration for each compound were obtained in sextuplicate. IC_{50} values were calculated using a nonlinear regression model (Binding/Saturation, one site−total) in GraphPad Prism 5.04.

PET Scanning and Biodistribution of U87MG Tumor Bearing Animals. All animal experiments with U87MG tumor bearing animals were performed with approval from the Peter MacCallum animal experimentation ethics committee. Six- to eight-week-old female Balb/c nude mice (Animal Resources Centre, Western Australia) were implanted subcutaneously on the right flank with 4 million U87MG cells. Once the tumors reached a volume >250 mm^3 (two to three weeks) the animals were injected intravenously with 13−30 MBq of [^{68}Ga(HP$_3$-RGD)] (1 μg of conjugate), [^{68}Ga(HP$_3$-RGD$_3$)] (2 μg of conjugate), and [^{68}Ga(HP$_9$-RGD$_3$)] (1 μg of conjugate) (100 μL of solutions described above). At 1 and 2 h, the animals were anaesthetized and imaged on a Philips MOSAIC small animal PET scanner for 10 min each. For blocking studies, animals were coinjected with c(RGDfK) peptide (400 μg), anaesthetized at 1 h, and imaged for 10 min each. The images were reconstructed using a 3D RAMLA algorithm, and radiotracer uptake was determined by ex vivo tissue counting as described previously.[70] On completion of the scan animals were euthanized by cervical dislocation and tissues harvested, weighed, and radioactivity counted using a gamma counter (Biomedex). Confidence intervals and p values were calculated using a two-tailed t-test in GraphPad Prism 5.04.

PET/CT Scanning and Biodistribution of Animals with Induced Rheumatoid Arthritis. All animal experiments on mice with induced rheumatoid arthritis complied with the Animals (Scientific Procedures) Act (UK 1986) and Home Office (UK) guidelines. A K/BxN serum transfer model of arthritis was utilized in these experiments, and serum was produced as previously reported.[59,60] Wild type C57Bl/6 male 6−8-week-old mice (Charles River) were injected with 150 μL arthritogenic serum (intraperitoneally) on days 0 and 2. The arthritic serum was either diluted 2-fold with PBS (to induce severe arthritis) or 8-fold with PBS (to induce mild arthritis). PBS alone was also injected into a third group to assess uptake in nonarthritic mice. Disease severity was evaluated in mice on days 0, 2 and 8 post-injection, by measuring weight loss, thickness of swollen paws, using microcalipers (Kroeplin), and visual clinical scoring on a scale of 0−3 per paw added for a

DOI: 10.1021/acs.bioconjchem.6b00621
Bioconjugate Chem. 2017, 28, 481−495

total score out of 12 per animal. On day 8, animals from the control, the mild arthritis and severe arthritis groups (n = 3) were injected intravenously with [^{68}Ga(HP$_3$-RGD$_3$)] (8−14 MBq, 4 μg HP$_3$-RGD$_3$). A fourth group of animals (n = 3) with severe arthritis were coadministered [^{68}Ga(HP$_3$-RGD$_3$)] (8−14 MBq, 4 μg HP$_3$-RGD$_3$) and c(RGDfK) peptide (400 μg). [^{68}Ga(HP$_3$-RGD$_3$)] was prepared using protocols described above for radiolabeling with an Eckert and Ziegler ^{68}Ge/^{68}Ga generator. Animals were injected under isoflurane anesthesia, after which they were immediately allowed to recover. One hour post-injection, animals were culled by CO_2 asphyxiation and PET scanned using a nanoScanPET/CT (Mediso Medical Imaging Systems, Budapest, Hungary) and organs/tissues harvested, weighed, and radioactivity counted using a gamma counter. PET/CT images were reconstructed using VivoQuant (inviCRO, LLC, Boston, USA). Confidence intervals and p values were calculated using a two-tailed t-test in GraphPad Prism 5.04.

■ ASSOCIATED CONTENT

Supporting Information

The Supporting Information is available free of charge on the ACS Publications website at DOI: 10.1021/acs.bioconjchem.6b00621.

Concentration response curves for solid-phase binding assay, ex vivo biodistribution data (PDF)

■ AUTHOR INFORMATION

Corresponding Author

*E-mail: michelle.ma@kcl.ac.uk.

ORCID

Michelle T. Ma: 0000-0002-3349-7346

Author Contributions

C.I. undertook synthesis and radiolabeling, and coauthored the manuscript; C.C. and R.J.H. conceived of and/or undertook PET imaging and biodistribution studies on U87MG cancer mouse models; S.Y.A.T., F.C., G.H.C., N.K.R., and A.P.C. conceived and/or undertook PET/CT and biodistribution studies on rheumatoid arthritis mouse models; P.R. assisted with radiolabeling; P.J.B. jointly conceived the study, advised on experimental methods and coauthored the manuscript; M.T.M. conceived the study, coauthored the manuscript, undertook synthesis, radiolabeling, LCMS analysis, and competitive binding assays, and conceived of and assisted with biodistribution studies. All authors have given approval to the final version of the manuscript.

Notes

The authors declare no competing financial interest.

■ ACKNOWLEDGMENTS

M.T.M. acknowledges the support of the People Programme (Marie Curie Actions) of the European Union's Seventh Framework Programme (FP7/2007-2013) under REA grant agreement number 299009, and the Royal Society of Chemistry through a Researcher Mobility Fellowship. C.I. acknowledges the NIHR Biomedical Research Centre for a PhD studentship. G.H.C., F.C., and A.P.C. acknowledge the support of Arthritis Research UK under grant number 20525. We thank Wayne Noonan, Kerry Ardley, and Rachael Walker for expert technical support. We thank Cristina Sanchez-Blanco for collecting the arthritogenic serum from KRN+ x NOD offspring. This research was supported by the Centre of Excellence in Medical Engineering Centre funded by the Wellcome Trust and EPSRC (WT088641/Z/09/Z), the KCL and UCL Comprehensive Cancer Imaging Centre funded by CRUK and EPSRC in association with the MRC and DoH (England), and by the NIHR Biomedical Research Centre at Guy's and St Thomas' NHS Foundation Trust and King's College London. The views expressed are those of the author(s) and not necessarily those of the NHS, the NIHR, or the DoH.

■ ABBREVIATIONS

HPLC, high performance liquid chromatography; HATU, 1,2-(7-aza-1H-benzotriazole-1-yl)-1,1,3,3-tetramethyluronium hexafluorophosphate; PET, positron emission tomography; TIC, total ion count

■ REFERENCES

(1) Hofman, M. S., Kong, G., Neels, O. C., Eu, P., Hong, E., and Hicks, R. J. (2012) High management impact of Ga-68 DOTATATE (GaTate) PET/CT for imaging neuroendocrine and other somatostatin expressing tumours. *J. Med. Imaging Radiat. Oncol. 56*, 40−7.

(2) Ambrosini, V., Campana, D., Tomassetti, P., and Fanti, S. (2012) ^{68}Ga-labelled peptides for diagnosis of gastroenteropancreatic NET. *Eur. J. Nucl. Med. Mol. Imaging 39* (Suppl 1), S52−60.

(3) Srirajaskanthan, R., Kayani, I., Quigley, A. M., Soh, J., Caplin, M. E., and Bomanji, J. (2010) The role of ^{68}Ga-DOTATATE PET in patients with neuroendocrine tumors and negative or equivocal findings on ^{111}In-DTPA-octreotide scintigraphy. *J. Nucl. Med. 51*, 875−82.

(4) Afshar-Oromieh, A., Zechmann, C. M., Malcher, A., Eder, M., Eisenhut, M., Linhart, H. G., Holland-Letz, T., Hadaschik, B. A., Giesel, F. L., Debus, J., and Haberkorn, U. (2014) Comparison of PET imaging with a ^{68}Ga-labelled PSMA ligand and ^{18}F-choline-based PET/CT for the diagnosis of recurrent prostate cancer. *Eur. J. Nucl. Med. Mol. Imaging 41*, 11−20.

(5) Fendler, W. P., Schmidt, D. F., Wenter, V., Zach, C., Bartenstein, P., Gildehaus, F. J., Thierfelder, K. M., Stief, C., Gratzke, C., Kirchner, T., and Faber, C. (2016) ^{68}Ga-PSMA-HBED-CC PET/CT detects location and extent of primary prostate cancer. *J. Nucl. Med. 57*, 1720−1725.

(6) Simecek, J., Notni, J., Kapp, T. G., Kessler, H., and Wester, H.-J. (2014) Benefits of NOPO as chelator in gallium-68 peptides, exemplified by preclinical characterization of ^{68}Ga-NOPO-c(RGDfK). *Mol. Pharmaceutics 11*, 1687−95.

(7) Boros, E., Ferreira, C. L., Yapp, D. T. T., Gill, R. K., Price, E. W., Adam, M. J., and Orvig, C. (2012) RGD conjugates of the H$_2$dedpa scaffold: synthesis, labeling and imaging with ^{68}Ga. *Nucl. Med. Biol. 39*, 785−94.

(8) Knetsch, P. A., Zhai, C., Rangger, C., Blatzer, M., Haas, H., Kaeopookum, P., Haubner, R., and Decristoforo, C. (2015) [^{68}Ga]-FSC-(RGD)$_3$ a trimeric RGD peptide for imaging $\alpha_v\beta_3$ integrin expression based on a novel siderophore derived chelating scaffold-synthesis and evaluation. *Nucl. Med. Biol. 42*, 115−22.

(9) Seemann, J., Waldron, B. P., Roesch, F., and Parker, D. (2015) Approaching 'kit-type' labelling with ^{68}Ga: the DATA chelators. *ChemMedChem 10*, 1019−26.

(10) Velikyan, I., Maecke, H., and Langstrom, B. (2008) Convenient preparation of ^{68}Ga-based PET-radiopharmaceuticals at room temperature. *Bioconjugate Chem. 19*, 569−73.

(11) Ferreira, C. L., Yapp, D. T. T., Mandel, D., Gill, R. K., Boros, E., Wong, M. Q., Jurek, P., and Kiefer, G. E. (2012) ^{68}Ga small peptide imaging: comparison of NOTA and PCTA. *Bioconjugate Chem. 23*, 2239−46.

(12) Ma, M. T., Neels, O. C., Denoyer, D., Roselt, P., Karas, J. A., Scanlon, D. B., White, J. M., Hicks, R. J., and Donnelly, P. S. (2011) Gallium-68 complex of a macrobicyclic cage amine chelator tethered to

DOI: 10.1021/acs.bioconjchem.6b00621
Bioconjugate Chem. 2017, 28, 481−495

two integrin-targeting peptides for diagnostic tumor imaging. *Bioconjugate Chem. 22*, 2093−103.
(13) Berry, D. J., Ma, Y., Ballinger, J. R., Tavare, R., Koers, A., Sunassee, K., Zhou, T., Nawaz, S., Mullen, G. E. D., Hider, R. C., and Blower, P. J. (2011) Efficient bifunctional gallium-68 chelators for positron emission tomography: tris(hydroxypyridinone) ligands. *Chem. Commun. 47*, 7068−70.
(14) Ma, M. T., Meszaros, L. K., Paterson, B. M., Berry, D. J., Cooper, M. S., Ma, Y., Hider, R. C., and Blower, P. J. (2015) Tripodal tris(hydroxypyridinone) ligands for immunoconjugate PET imaging with $^{89}Zr^{4+}$: comparison with desferrioxamine-B. *Dalton Trans. 44*, 4884−900.
(15) Chaves, S., Mendonca, A. C., Marques, S. M., Prata, M. I., Santos, A. C., Martins, A. F., Geraldes, C. F. G. C., and Santos, M. A. (2011) A gallium complex with a new tripodal tris-hydroxypyridinone for potential nuclear diagnostic imaging: solution and in vivo studies of ^{67}Ga-labeled species. *J. Inorg. Biochem. 105*, 31−38.
(16) Chaves, S., Marques, S. M., Matos, A. M. F., Nunes, A., Gano, L., Tuccinardi, T., Martinelli, A., and Santos, M. A. (2010) New tris(hydroxypyridinones) as iron and aluminium sequestering agents: synthesis, complexation and in vivo studies. *Chem. - Eur. J. 16*, 10535−45.
(17) Zhou, T., Neubert, H., Liu, D. Y., Liu, Z. D., Ma, Y. M., Kong, X. L., Luo, W., Mark, S., and Hider, R. C. (2006) Iron binding dendrimers: a novel approach for the treatment of hemochromatosis. *J. Med. Chem. 49*, 4171−82.
(18) Ma, M. T., Cullinane, C., Imberti, C., Baguna Torres, J., Terry, S. Y. A., Roselt, P., Hicks, R. J., and Blower, P. J. (2016) New tris(hydroxypyridinone) bifunctional chelators containing isothiocyanate groups provide a versatile platform for rapid one-step labeling and PET imaging with $^{68}Ga^{3+}$. *Bioconjugate Chem. 27*, 309−18.
(19) Ma, M. T., Cullinane, C., Waldeck, K., Roselt, P., Hicks, R. J., and Blower, P. J. (2015) Rapid kit-based ^{68}Ga-labelling and PET imaging with THP-Tyr^3-octreotate: a preliminary comparison with DOTA-Tyr^3-octreotate. *EJNMMI Res. 5*, 52.
(20) Cao, F., Li, Z., Lee, A., Liu, Z., Chen, K., Wang, H., Cai, W., Chen, X., and Wu, J. C. (2009) Noninvasive de novo imaging of human embryonic stem cell-derived teratoma formation. *Cancer Res. 69*, 2709−13.
(21) Terry, S. Y. A., Abiraj, K., Frielink, C., van Dijk, L. K., Bussink, J., Oyen, W. J., and Boerman, O. C. (2014) Imaging integrin $\alpha_v\beta_3$ on blood vessels with ^{111}In-RGD$_2$ in head and neck tumor xenografts. *J. Nucl. Med. 55*, 281−86.
(22) Hernandez, R., Valdovinos, H. F., Yang, Y., Chakravarty, R., Hong, H., Barnhart, T. E., and Cai, W. (2014) ^{44}Sc: an attractive isotope for peptide-based PET imaging. *Mol. Pharmaceutics 11*, 2954−61.
(23) Liu, S., Liu, Z., Chen, K., Yan, Y., Watzlowik, P., Wester, H.-J., Chin, F. T., and Chen, X. (2010) ^{18}F-labeled galacto and PEGylated RGD dimers for PET imaging of $\alpha_v\beta_3$ integrin expression. *Mol. Imaging Biol. 12*, 530−8.
(24) Dijkgraaf, I., Terry, S. Y. A., McBride, W. J., Goldenberg, D. M., Laverman, P., Franssen, G. M., Oyen, W. J. G., and Boerman, O. C. (2013) Imaging integrin alpha-v-beta-3 expression in tumors with an ^{18}F-labeled dimeric RGD peptide. *Contrast Media Mol. Imaging 8*, 238−45.
(25) Oxboel, J., Brandt-Larsen, M., Schjoeth-Eskesen, C., Myschetzky, R., El-Ali, H. H., Madsen, J., and Kjaer, A. (2014) Comparison of two new angiogenesis PET tracers ^{68}Ga-NODAGA-E[c(RGDyK)]$_2$ and ^{64}Cu-NODAGA-E[c(RGDyK)]$_2$; in vivo imaging studies in human xenograft tumors. *Nucl. Med. Biol. 41*, 259−67.
(26) Wangler, C., Maschauer, S., Prante, O., Schafer, M., Schirrmacher, R., Bartenstein, P., Eisenhut, M., and Wangler, B. (2010) Multimerization of cRGD peptides by click chemistry: synthetic strategies, chemical limitations, and influence on biological properties. *ChemBioChem 11*, 2168−81.
(27) Notni, J., Pohle, K., and Wester, H.-J. (2013) Be spoilt for choice with radiolabelled RGD peptides: preclinical evaluation of ^{68}Ga-TRAP(RGD)$_3$. *Nucl. Med. Biol. 40*, 33−41.
(28) Martinelli, J., Thangavel, K., Tei, L., and Botta, M. (2014) Dendrimeric β-cyclodextrin/Gd(III) chelate supramolecular host-guest adducts as high-relaxivity MRI probes. *Chem. - Eur. J. 20*, 10944−52.
(29) Bryson, J. M., Chu, W.-J., Lee, J.-H., and Reineke, T. M. (2008) A β-cyclodextrin "Click cluster" decorated with seven paramagnetic chelates containing two water exchange sites. *Bioconjugate Chem. 19*, 1505−09.
(30) Mastarone, D. J., Harrison, V. S. R., Eckermann, A. L., Parigi, G., Luchinat, C., and Meade, T. J. (2011) A modular system for the synthesis of multiplexed magnetic resonance probes. *J. Am. Chem. Soc. 133*, 5329−37.
(31) Moore, J. D., and Allen, M. J. (2011) Multilanthanide systems for medical imaging applications. *Recent Pat. Nanomed. 1*, 88−100.
(32) Wiener, E., and Narayanan, V. V. (2002) *Advances in Dendritic Macromolecules. Vol. 5: Magnetic resonance imaging contrast agents: theory and the role of dendrimers* (Newkome, G. R., Ed.) pp 129−247, Chapter 4, Elsevier.
(33) Zhao, G., Lu, C., Li, H., Xiao, Y., Zhang, W., Fang, X., Wang, P., Fang, X., Xu, J., and Yang, W. (2013) Two multinuclear Gd^{III} macrocyclic complexes as contrast agents with high relaxivity and stability using rigid linkers. *Inorg. Chim. Acta 406*, 146−52.
(34) Fontes, A., Karimi, S., Helm, L., Yulikov, M., Ferreira, P. M., and Andre, J. P. (2015) Dinuclear DOTA-based Gd^{III} chelates - revisiting a straightforward strategy for relaxivity improvement. *Eur. J. Inorg. Chem. 2015*, 1579−91.
(35) Gugliotta, G., Botta, M., and Tei, L. (2010) AAZTA-based bifunctional chelating agents for the synthesis of multimeric/dendrimeric MRI contrast agents. *Org. Biomol. Chem. 8*, 4569−74.
(36) Ranganathan, R. S., Fernandez, M. E., Kang, S. I., Nunn, A. D., Ratsep, P. C., Pillai, K. M. R., Zhang, X., and Tweedle, M. F. (1998) New multimeric magnetic resonance imaging agents. *Invest. Radiol. 33*, 779−97.
(37) Valdes, O., Vergara, C. E., Camarada, M. B., Carrasco-Sanchez, V., Nachtigall, F. M., Tapia, J., Fischer, R., Gonzalez-Nilo, F. D., and Santos, L. S. (2015) Synthesis and characterization of an insoluble polymer based on polyamidoamine: applications for the decontamination of metals in aqueous systems. *J. Environ. Manage. 147*, 321−29.
(38) Kobayashi, H., Sato, N., Saga, T., Nakamoto, Y., Ishimori, T., Toyama, S., Togashi, K., Konishi, J., and Brechbiel, M. W. (2000) Monoclonal antibody-dendrimer conjugates enable radiolabeling of antibody with markedly high specific activity with minimal loss of immunoreactivity. *Eur. J. Nucl. Med. 27*, 1334−39.
(39) Kobayashi, H., Wu, C., Kim, M.-K., Paik, C. H., Carrasquillo, J. A., and Brechbiel, M. W. (1999) Evaluation of the in vivo biodistribution of indium-111 and yttrium-88 labeled dendrimer-1B4M-DTPA and its conjugation with anti-tac monoclonal antibody. *Bioconjugate Chem. 10*, 103−11.
(40) Waengler, C., Moldenhauer, G., Eisenhut, M., Haberkorn, U., and Mier, W. (2008) Antibody-dendrimer conjugates: the number, not the size of the dendrimers, determines the immunoreactivity. *Bioconjugate Chem. 19*, 813−20.
(41) Wu, C., Brechbiel, M. W., Kozak, R. W., and Gansow, O. A. (1994) Metal-chelate-dendrimer-antibody constructs for use in radioimmunotherapy and imaging. *Bioorg. Med. Chem. Lett. 4*, 449−54.
(42) Grunberg, J., Jeger, S., Sarko, D., Dennler, P., Zimmermann, K., Mier, W., and Schibli, R. (2013) DOTA-functionalized polylysine: a high number of DOTA chelates positively influences the biodistribution of enzymatic conjugated anti-tumor antibody chCE7agl. *PLoS One 8*, e60350.
(43) Ramli, M., Smith, S. V., and Lindoy, L. F. (2009) Investigation of novel bis- and tris-tetraazamacrocycles for use in the copper-64 (^{64}Cu) radiolabeling of antibodies with potential to increase the therapeutic index for drug targeting. *Bioconjugate Chem. 20*, 868−76.
(44) Slinkin, M. A., Klibanov, A. L., Khaw, B. A., and Torchilin, V. P. (1990) Succinylated polylysine as a possible link between an antibody molecule and deferoxamine. *Bioconjugate Chem. 1*, 291−5.
(45) Lee, H.-Y., Li, Z., Chen, K., Hsu, A. R., Xu, C., Xie, J., Sun, S., and Chen, X. (2008) PET/MRI dual-modality tumor imaging using

DOI: 10.1021/acs.bioconjchem.6b00621
Bioconjugate Chem. 2017, 28, 481−495

arginine-glycine-aspartic (RGD)-conjugated radiolabeled iron oxide nanoparticles. *J. Nucl. Med. 49*, 1371−79.
(46) Frigell, J., Garcia, I., Gomez-Vallejo, V., Llop, J., and Penades, S. (2014) ^{68}Ga-Labeled gold glyconanoparticles for exploring blood-brain barrier permeability: preparation, biodistribution studies, and improved brain uptake via neuropeptide conjugation. *J. Am. Chem. Soc. 136*, 449−57.
(47) Lee, J., Lee, T. S., Ryu, J., Hong, S., Kang, M., Im, K., Kang, J. H., Lim, S. M., Park, S., and Song, R. (2013) RGD peptide-conjugated multimodal $NaGdF_4$:Yb^{3+}/Er^{3+} nanophosphors for upconversion luminescence, MR, and PET imaging of tumor angiogenesis. *J. Nucl. Med. 54*, 96−103.
(48) Lee, S., Kang, S.-W., Ryu, J. H., Na, J. H., Lee, D.-E., Han, S. J., Kang, C. M., Choe, Y. S., Lee, K. C., Leary, J. F., Choi, K., Lee, K.-H., and Kim, K. (2014) Tumor-homing glycol chitosan-based optical/PET dual imaging nanoprobe for cancer diagnosis. *Bioconjugate Chem. 25*, 601−10.
(49) Zhernosekov, K. P., Filosofov, D. V., Baum, R. P., Aschoff, P., Bihl, H., Razbash, A. A., Jahn, M., Jennewein, M., and Roesch, F. (2007) Processing of generator-produced ^{68}Ga for medical application. *J. Nucl. Med. 48*, 1741−48.
(50) Eppard, E., Wuttke, M., Nicodemus, P. L., and Roesch, F. (2014) Ethanol-based post-processing of generator-derived ^{68}Ga toward kit-type preparation of ^{68}Ga-radiopharmaceuticals. *J. Nucl. Med. 55*, 1023−28.
(51) Li, Z.-b., Cai, W., Cao, Q., Chen, K., Wu, Z., He, L., and Chen, X. (2007) ^{64}Cu-labeled tetrameric and octameric RGD peptides for small-animal PET of tumor $\alpha_v\beta_3$ integrin expression. *J. Nucl. Med. 48*, 1162−71.
(52) Kerr, J. S., Slee, A. M., and Mousa, S. A. (2000) Small molecule α_v integrin antagonists: novel anticancer agents. *Expert Opin. Invest. Drugs 9*, 1271−79.
(53) Wilder, R. L. (2002) Integrin alpha V beta 3 as a target for treatment of rheumatoid arthritis and related rheumatic diseases. *Ann. Rheum. Dis. 61*, 96−99.
(54) Maracle, C. X., and Tas, S. W. (2014) Inhibitors of angiogenesis: ready for prime time? *Best Pract. Res. Clin. Rheumatol. 28*, 637−49.
(55) Terry, S. Y. A., Koenders, M., Franssen, G., Nayak, T., Freimoser-Grundschober, A., Klein, C., Oyen, W., Boerman, O., and Laverman, P. (2016) Monitoring therapy response of experimental arthritis with radiolabeled tracers targeting fibroblasts, macrophages or integrin $\alpha_v\beta_3$. *J. Nucl. Med. 57*, 467−72.
(56) Huang, C., Zheng, Q., and Miao, W. (2015) Study of novel molecular probe ^{99m}Tc-3PRGD$_2$ in the diagnosis of rheumatoid arthritis. *Nucl. Med. Commun. 36*, 1208−14.
(57) Zhu, Z., Yin, Y., Zheng, K., Li, F., Chen, X., Zhang, F., and Zhang, X. (2014) Evaluation of synovial angiogenesis in patients with rheumatoid arthritis using ^{68}Ga-PRGD$_2$ PET/CT: a prospective proof-of-concept cohort study. *Ann. Rheum. Dis. 73*, 1269−72.
(58) Zheleznyak, A., Wadas, T. J., Sherman, C. D., Wilson, J. M., Kostenuik, P. J., Weilbaecher, K. N., and Anderson, C. J. (2012) Integrin $\alpha_v\beta_3$ as a PET imaging biomarker for osteoclast number in mouse models of negative and positive osteoclast regulation. *Mol. Imaging Biol. 14*, 500−8.
(59) Kouskoff, V., Korganow, A.-S., Duchatelle, V., Degott, C., Benoist, C., and Mathis, D. (1996) Organ-specific disease provoked by systemic autoimmunity. *Cell 87*, 811−22.
(60) Monach, P. A., Mathis, D., and Benoist, C. (2008) The K/BxN arthritis model. In *Current Protocols in Immunogy*, Chapter 15, Unit 15.22, DOI: 10.1002/0471142735.im1522s81
(61) Chen, X., Liu, S., Hou, Y., Tohme, M., Park, R., Bading, J., and Conti, P. (2004) MicroPET imaging of breast cancer α_v-integrin expression with ^{64}Cu-labeled dimeric RGD peptides. *Mol. Imaging Biol. 6*, 350−9.
(62) Shi, J., Kim, Y.-S., Zhai, S., Liu, Z., Chen, X., and Liu, S. (2009) Improving tumor uptake and pharmacokinetics of ^{64}Cu-labeled cyclic RGD peptide dimers with Gly$_3$ and PEG$_4$ linkers. *Bioconjugate Chem. 20*, 750−59.
(63) Liu, Z., Niu, G., Shi, J., Liu, S., Wang, F., Liu, S., and Chen, X. (2009) ^{68}Ga-labeled cyclic RGD dimers with Gly$_3$ and PEG$_4$ linkers: promising agents for tumor integrin $\alpha_v\beta_3$ PET imaging. *Eur. J. Nucl. Med. Mol. Imaging 36*, 947−57.
(64) Dijkgraaf, I., Yim, C.-B., Franssen, G. M., Schuit, R. C., Luurtsema, G., Liu, S., Oyen, W. J. G., and Boerman, O. C. (2011) PET imaging of $\alpha_v\beta_3$ integrin expression in tumours with ^{68}Ga-labelled mono-, di- and tetrameric RGD peptides. *Eur. J. Nucl. Med. Mol. Imaging 38*, 128−37.
(65) Li, Z.-B., Chen, K., and Chen, X. (2008) ^{68}Ga-labeled multimeric RGD peptides for microPET imaging of integrin $\alpha_v\beta_3$ expression. *Eur. J. Nucl. Med. Mol. Imaging 35*, 1100−08.
(66) Li, Z.-b., Cai, W., Cao, Q., Chen, K., Wu, Z., He, L., and Chen, X. (2007) ^{64}Cu-labeled tetrameric and octameric RGD peptides for small-animal PET of tumor $\alpha_v\beta_3$ integrin expression. *J. Nucl. Med. 48*, 1162−71.
(67) Put, S., Westhovens, R., Lahoutte, T., and Matthys, P. (2014) Molecular imaging of rheumatoid arthritis: emerging markers, tools, and techniques. *Arthritis Res. Ther. 16*, 208.
(68) Matteson, E. L., Lowe, V. J., Prendergast, F. G., Crowson, C. S., Moder, K. G., Morgenstern, D. E., Messmann, R. A., and Low, P. S. (2009) Assessment of disease activity in rheumatoid arthritis using a novel folate targeted radiopharmaceutical Folatescan. *Clin. Exp. Rheumatol. 27*, 253−9.
(69) Liu, Z. D., Kayyali, R., Hider, R. C., Porter, J. B., and Theobald, A. E. (2002) Design, synthesis, and evaluation of novel 2-substituted 3-hydroxypyridin-4-ones: Structure-activity investigation of metalloenzyme inhibition by iron chelators. *J. Med. Chem. 45*, 631−39.
(70) Paterson, B. M., Roselt, P., Denoyer, D., Cullinane, C., Binns, D., Noonan, W., Jeffery, C. M., Price, R. I., White, J. M., Hicks, R. J., and Donnelly, P. S. (2014) PET imaging of tumours with a ^{64}Cu labeled macrobicyclic cage amine ligand tethered to Tyr$_3$-octreotate. *Dalton Trans. 43*, 1386−96.

DOI: 10.1021/acs.bioconjchem.6b00621
Bioconjugate Chem. 2017, 28, 481−495